

**TREE SPECIES CLASSIFICATION
USING SEASONAL UAV-RGB DATA,
SUMMER UAV MULTI-SPECTRAL
DATA, AND ITS COMBINATION IN A
MIXED TEMPERATE FOREST: A
CASE STUDY OF HAAGSE BOS,
NETHERLANDS.**

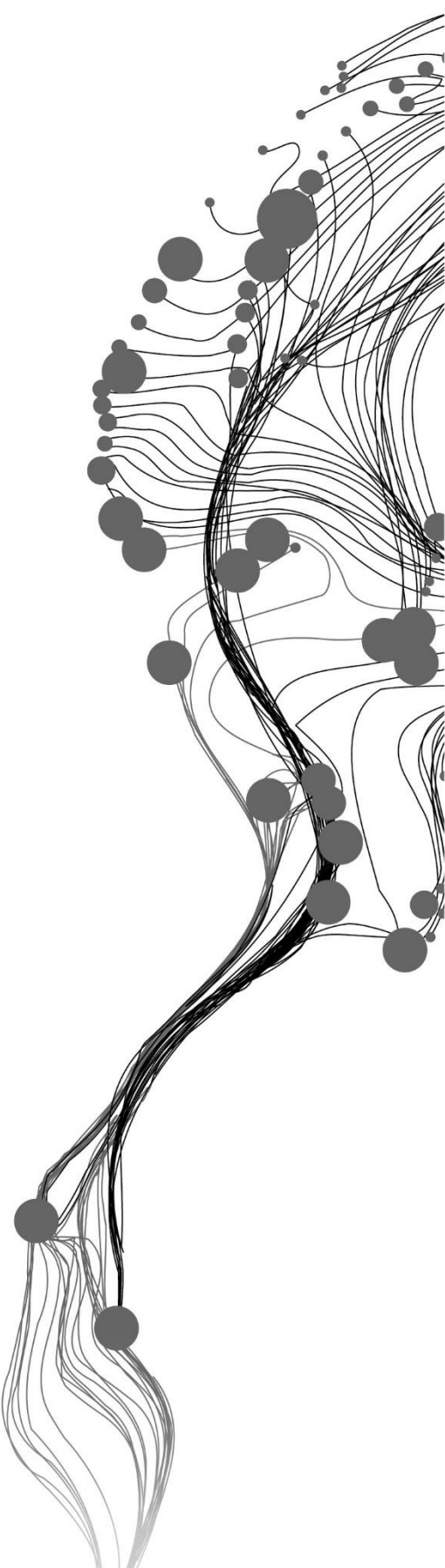
EFIA BOAKYE ADDO

August 2020

SUPERVISORS:

Ir. L.M. Van Leeuwen- de Leeuw (First supervisor)

Drs. Ing. M. Huesca Martinez (Second supervisor)



TREE SPECIES CLASSIFICATION USING SEASONAL UAV-RGB DATA, SUMMER UAV MULTI-SPECTRAL DATA, AND ITS COMBINATION IN A MIXED TEMPERATE FOREST: A CASE STUDY OF HAAGSE BOS, NETHERLANDS.

EFIA BOAKYE ADDO

Enschede, The Netherlands, August 2020

Thesis submitted to the Faculty of Geo-Information Science and Earth Observation of the University of Twente in partial fulfilment of the requirements for the degree of Master of Science in Geo-information Science and Earth Observation.

Specialization: Natural Resource Management

SUPERVISORS:

Ir. L.M. Van Leeuwen- de Leeuw (First supervisor)

Drs. Ing. M. Huesca Martinez (Second supervisor)

THESIS ASSESSMENT BOARD:

Dr. R. Darvish (Chair)

Dr. Tuomo Kauranne (External Examiner, Lappeenranta University of Technology, Finland)

DISCLAIMER

This document describes work undertaken as part of a programme of study at the Faculty of Geo-Information Science and Earth Observation of the University of Twente. All views and opinions expressed therein remain the sole responsibility of the author, and do not necessarily represent those of the Faculty.

ABSTRACT

Tree species classification is of importance to various groups of people who manage and protect the forest. While some forest managers need this information to undertake the appropriate silvicultural activities, others need this information to identify tree species that can be harvested for timber. Tree species information can be used to identify and conserve endangered species, indicates biodiversity richness, and is also used to identify a species-specific allometric equation to estimate forest biomass and carbon. Although tree species information can be obtained at any time, the tree's phenological changes make it possible to identify certain tree species better in a specific season than the others.

In view of this, this research aimed to compare the results of classification of tree species using seasonal UAV-RGB images, summer UAV-MSS images, and its combination in a temperate forest. The object-based image analysis and support vector machine classification algorithm was deployed to classify eight tree species and a combination of tree species named others. The tree crowns were first identified using multi-resolution segmentation (MRS) algorithm in object-based image analysis. The accuracy of the tree crowns was assessed by estimating the under segmentation, over-segmentation, and overall segmentation error. The generated tree crowns, combined with tree species data collected from the field, were used to classify the seasonal UAV-RGB datasets, summer UAV-MSS dataset, and the combination of summer UAV-RGB and MSS datasets using a support vector machine classification algorithm. The accuracy of the tree species classification was then assessed by generating the confusion matrix.

The summer MSS dataset produced a segmentation accuracy of 82%, which was the highest among the other seasonal dataset. The summer RGB, fall RGB, summer MSS and RGB, spring, and winter RGB yielded segmentation accuracy of 76%, 73%, 71%, 57%, and 31%, respectively. The result of the tree species classification showed that the summer UAV-RGB dataset resulted in the highest classification accuracy of 0.77 compared to the winter, fall, and spring UAV-RGB datasets, resulting in the overall accuracy of 0.49, 0.68, and 0.64, respectively. The summer UAV-MSS dataset yielded an overall accuracy of 0.84, while the combination of summer UAV-RGB and MSS yielded the best overall accuracy of 0.88. This research suggests that combining UAV-RGB and MSS datasets of the same season can improve tree species classification, better estimating species-level above-ground biomass and sustainable management of natural resources.

Keywords: UAV-RGB, UAV-MSS, object-based image analysis, support vector machine, tree species, user accuracy, producer accuracy, overall accuracy, F measure, kappa, Haagse Bos.

ACKNOWLEDGEMENTS

My greatest thanks and appreciation to the Almighty God who has granted me the gift of life and good health throughout my life. Without God, it would not have been possible to pursue and complete this programme. I thank the International Christian Fellowship (ICF) for creating an atmosphere to reignite my love for God.

I take this opportunity to thank the Netherlands Government and the Orange Knowledge Programme (OKP) for the scholarship granted that caters for all financial costs making it possible to concentrate on just the academics.

My genuine and most gratitude goes to my first and second supervisor Ms Ir. L.M. van Leeuwen – de Leeuw and Drs. Ing. M. Huesca Martinez for their kind heart, patience, encouragement, and advice throughout the research. It was fun working with you both, and I learnt a lot. To Tim Roberts, I am grateful for taking the time to help me acquire my UAV images for this research. To the whole staff of the Faculty of Geo-Information Science and Earth Observation (ITC), I thank you for the knowledge I gained throughout my stay.

Special thanks go to Haagse Bos management and community for giving us permission to conduct our UAV flight and carry out a data collection exercise in the forest. To add, many thanks to Takkenkamp company manager Mr. Teun Schoolkate, who took his time to take us around the forest and understand the challenges they face as forest managers and managing the forest.

Likewise, I would like to convey my thanks to the team I worked with during data collection, also to the fantastic friends I made at the Faculty of ITC and the NRS 2019-2021 group. It was terrific spending 24 months with you guys and my work was made easier with your support and encouragement.

My sincere gratitude to Mr Ofori Lartey whose encouragement and unconditional support got me into starting this academic adventure, and likewise goes to Etse Lossou for being there all the time from start to finish of my programme at ITC. Mainly I also feel profoundly grateful to Clement Obeng Manu for his support and valuable feedbacks.

Finally, to my mother, father, and siblings, I am also grateful for the love and support and the push you gave me in these 24 months of my academic journey.

TABLE OF CONTENTS

1.	INTRODUCTION	8
1.1.	Background.....	8
1.2.	Problem statement.....	12
1.3.	Research objectives.....	13
1.4.	Research questions.....	13
1.5.	Conceptual diagram	13
2.	STUDY AREA, MATERIALS, AND METHOD	15
2.1.	Study area.....	15
2.2.	Material.....	16
2.3.	Method.....	17
2.4.	Fieldwork.....	17
2.5.	Data processing.....	21
2.6.	Data analysis.....	23
3.	RESULTS.....	34
3.1.	Segmentation of images.....	34
3.2.	Tree species classification	35
3.3.	Accuracy assessment.....	41
4.	DISCUSSION	43
4.1.	Segmentation accuracy of the seasonal dataset.....	43
4.2.	Tree species classification of UAV-RGB dataset	46
4.3.	UAV- MSS for tree species classification	49
5.	CONCLUSION AND RECOMMENDATION	51
5.1.	Conclusion	51
5.2.	Recommendation.....	52

LIST OF FIGURES

Figure 1-1: Mean spectral signatures of 10 tree species.....	10
Figure 1-2: A deciduous tree under different seasons	11
Figure 1-3: Conceptual diagram of system interactions	14
Figure 2-1: Map of the study area, Haagse Bos, Enschede.....	15
Figure 2-2: Flowchart of method.....	17
Figure 2-3: Sequoia camera mounted on DJI Phantom 4 Pro and AIRINOV target.....	18
Figure 2-4: Recording 3-D coordinate of GCP with DGNS RTK in an open space	19
Figure 2-5: Overlapping images observing the same features at different location.	21
Figure 2-6: Orthophoto of the summer, spring, fall, and winter dataset.....	22
Figure 2-7: Green, red, near infra-red, and red edge bands from the summer MSs dataset.	23
Figure 2-8: CHM of the summer, spring, fall, and winter dataset.	24
Figure 2-9: ESP result for fall RGB and summer MSS dataset.....	25
Figure 2-10: Ruleset for segmentation (in red) and classification with the resulting segment.	26
Figure 2-11: A mapping showing the manually digitised segments.....	26
Figure 2-12: Features for summer UAV-RGB dataset classification	29
Figure 2-13: Possible planes that can separate classes (a) and optimal plane that can separate classes.....	30
Figure 2-14: Projecting the training data into a high-dimensional feature space.	31
Figure 3-1: Segmentation output for UAV-RGB fall dataset.....	35
Figure 3-2: Summer UAV-RGB tree species classification	36
Figure 3-3: Winter UAV-RGB tree species classification	37
Figure 3-4: Winter UAV-RGB tree species classification	38
Figure 3-5: Fall UAV-RGB tree species classification.....	39
Figure 3-6: Summer UAV-MSS tree species classification	40
Figure 3-7: Tree species classification of fall UAV-RGB dataset.....	41
Figure 4-1: Pictorial view of some deciduous tree samples in the four seasons.....	43
Figure 4-2: Comparing MRS segments (blue) and manually digitized segment (red) for under segmentation and over-segmentation of tree crown.	44
Figure 4-3: Comparison of Summer RGB and MSS Red and Green dataset for some selected trees	45
Figure 4-4: Oak and beech profile of all features used for summer UAV-RGB dataset.....	46
Figure 4-5: Oak and beech profile of all features used for summer UAV-RGB dataset.....	46
Figure 4-6: Spectral profile of some features and tree species	47
Figure 4-7: Larch in spring, summer, fall and winter.....	48
Figure 4-8: Birch trees in winter.....	48
Figure 4-9: GLCM contrast spectral profile for tree species.....	49

LIST OF TABLES

Table 2-1: Field instruments and their use on the field.....	16
Table 2-2: Software and its uses	16
Table 2-3: UAV flight plan	19
Table 2-4: Data from previous studies	19
Table 2-5: Tree species and samples collected.....	20
Table 2-6: Parameters per seasonal dataset for SVM classification	32
Table 3-1: Segmentation parameters used for all seasonal datasets.....	34
Table 3-2: Segmentation accuracy of all input datasets	35
Table 3-3: Tree species classification accuracies for all datasets.	41
Table 3-4: F measure per tree species per seasonal dataset	42

LIST OF TACRONYMS

BBA	Bundle Block Adjustment
CHM	Canopy Height Model
DSM	Digital Surface Model
DTM	Digital Terrain Model
ESP	Estimation Scale Parameter
GCP	Ground control point
CHM	Canopy Height Model
GLCM	Gray Level Co-occurrence Matrix
GLDV	Gray Level Difference Vector
GNSS	Global Navigational Satellite System
GPS	Global Positioning System
OA	Overall accuracy
OBIA	Object-based image analysis
RANSAC	Random Sample Consensus
RBF	Radial kernel basis function
RGB	Red Green Blue
RMSE	Root Mean Square Error
SfM	Structure from Motion
SVM	Support Vector Machine
UA	User accuracy
UAV	Unmanned Aerial Vehicle

1. INTRODUCTION

1.1. Background

According to the Food and Agriculture Organization, a forest is an area of more than 0.5 hectares, with trees covering more than 10% (FAO, 2020). Forest provides beneficial services to humans and the environment. For example, wood obtained from the forest is a source of timber, energy, and fuel. Forest also plays a vital role in carbon sequestration, global warming, and biogeochemical cycles (Overpeck et al., 2005). While a growing forest absorbs carbon dioxide (CO₂) from the environment, degradation and deforestation of the forest raise the concentration of greenhouse gases (GHG) into the atmosphere.

Forest aids biodiversity conservation, providing habitat for both plants and animal species (Aerts & Honnay, 2011). Tropical rainforests are one of the most biodiversity-rich ecosystems globally, accommodating about 50-90% of all plant species (Angelsen, 2001). However, temperate forests comprising fewer tree species may also have high levels of biodiversity, especially when considering the various life forms (birds, plants, fungi, etc.). The different seasonality experienced per region influences tree species differently. Some tree species in the temperate forest respond differently to seasons by changing their leaf colour from green to yellow due to the loss of chlorophyll. It is also observed that while some trees lose their leaves in some seasons, other trees remain green through all the seasons. Seasonality influences biodiversity (Armstrong, 2010) as some of the sequential fluxes in the abundance of species are related to seasons (Shimadzu et al., 2013).

Biodiversity is the variability among life forms, including microorganisms, plants, and animals in different ecosystems, such as terrestrial, aquatic, marine, etc. (Schwenk et al., 2012). Various biodiversity hotspots can be found worldwide, with unique clustered plant species diversity (Gaston, 2000; Leyequien et al., 2007). Loss of biodiversity reduces species connectivity and damages the ecosystems, leading to the extinction of some species in local populations and the disruption of ecological services (Schwenk et al., 2012). On the other hand, species diversity often increases productivity, including biomass and carbon storage (Chen et al., 2018).

While biodiversity includes all life forms, tree species diversity at a particular location is a way to estimate the richness of tree species. However, acquiring complete information of tree species at a specific geographic area can be a complicated process. Although identifying tree species can be complex, it is essential to evaluate forest ecosystems and their related services as it helps protect, manage, and assess the resilience and vulnerability of the forest (Sheeren et al., 2016). Acquiring the exact location of a tree is essential to carry out biomass estimation using species-specific allometric equations. Biomass estimation using species information yields a better biomass estimate than using a generic allometric equation for carbon estimation. Tree species data can be obtained through field inventory, species distribution models (SDM's), or remote sensing data.

Field inventory is the best and accurate way to map tree species. However, field observations are costly in time, labour, and resources. Also, some areas may be inaccessible to field workers (Modzelewska et al., 2020). SDM's have also been used to derive maps of existing tree species. The maps from SDM's provide the probability of the presence of tree species within a geographic location but not the exact location of tree species (Modzelewska et al., 2020). SDM's forecast the species using habitat indicators and existing species data (Brus et al., 2012). The remote sensing approach is an alternative to field inventory and the SDM approach to map tree species. The remote sensing approach utilizes the statistical relationship that may exist

between the remote sensing data and the trees in the forest (Gibbs & Herold, 2007). Previously, studies that mapped tree species investigated the influence of spatial resolution of the remote sensing data (Nagendra, 2001). However, most of these studies used a pixel-based approach to classify the tree species (Franklin et al., 2000; Brandtberg, 2002; Erikson, 2004).

The traditional classification of satellite imagery is a pixel-based approach based on the probability that a particular pixel belongs to a defined class (Mather & Tso, 2016). The pixel-based process examines the image pixels spectral characteristics without considering the pixels spatial and contextual properties (Weih & Riggan, 2010). Using the traditional classification algorithms for medium and coarse resolution remote sensing images yields moderate classification results (Gao & Mas, 2008; Congalton & Green, 2019). However, using the traditional classification algorithms to classify very high resolution (VHR) remote sensing images results in the “salt and pepper” effects, leading to misclassification. The “salt and pepper” effect is due to the high variability implicit in VHR remote sensing images. Object-Based Image Analysis (OBIA) is the preferred option for analysing VHR remote sensing images. The OBIA is employed to detect individual objects in an image dataset. The object-based approach analyses the images’ spectral, spatial, and contextual properties to improve classification accuracy (Weih & Riggan, 2010). After obtaining the image objects, a classification algorithm including machine learning algorithms can be used to build a model for the classification task. Machine learning algorithms are algorithms that create models without explicit programming. The models developed are then used to make predictions. Machine learning algorithms identify the trends and patterns within the input data to continuously enhance the output model to improve predictions (Data-flair, 2020). Finally, the algorithm developed is used to classify the image objects acquired from the object-based approach to avoid the “salt and pepper” effect and improve the classification result. This is done by generating features from the input data to be included in the training and classifying of images.

Developments in satellite remote sensing technology led to very high spatial resolution (VHR) images. Also, advances made in machine learning resulted in further probes into species classification. Several researchers have coupled machine learning and VHR images to identify tree species in many geographical locations. For example, Viennois et al. (2016) used eight VHR satellite images (Ikonos, GeoEye, Quickbird, and Worldview 2) between 2001 and 2014 in a time series analysis to investigate the accuracy of satellite reflectance for tree species mapping in Bali, Indonesia and obtained accuracy between 66% and 80%. Wang et al. (2018) also used Pléiades-1 satellite images to classify tree species in Lingding Bay of the Pearl River Estuary, China. In their research, they combined OBIA and machine learning classification algorithms to classify Pléiades-1 data. They harnessed the potential of OBIA to extract image objects and compared support vector machine (SVM), random forest (RF) and decision tree (DT) machine learning algorithms to classify tree species to determine the classification algorithm among the tested algorithms. They reported an overall accuracy of 82%. Cho et al., (2015) used an SVM classifier for tree species classification using WorldView-2 images and identified three dominant tree species in the Dukuduku forest in South Africa, obtaining an accuracy of 89.3%.

Recent research uses Unmanned Aerial Vehicles (UAVs) to acquire high spatial and spectral resolution satellite images for forest mapping (Näsi et al., 2016; Nevalainen et al., 2017). UAV is a cost-effective way for data capturing and operates on user demand. UAV images are processed using a photogrammetric approach to produce 3-D point information from 2-D imagery. The 3-D points are used to generate orthophoto, Digital Surface Model (DSM), and Digital Terrain Model (DTM). The output of the photogrammetric workflow can be deployed to analyse and monitor forest ecosystems at preferred periods.

Xu et al. (2020) used a random forest classifier to classify tree species by combining multi-spectral, texture and point cloud metrics from the UAV dataset to delineate tree species. Their research resulted in an accuracy of 80.2% and identified eight dominant tree species. Eshetae (2020) also classified tree species using UAV-RGB images and support vector machine classifier algorithms in a Temperate Forest in the Netherlands to develop a model to classify tree species and reported a classification accuracy of 78%. Onishi & Ise (2018) also used UAV-RGB images captured in Kyoto, Japan and deep learning to classify seven dominant tree types and reported an accuracy of 89.0%.

UAVs can obtain a multi-spectral and multi-temporal dataset to identify the phenological changes in the tree life cycle. UAV-based multi-spectral data are beneficial for tree species discrimination as it includes bands such as near infra-red and red edge. Research indicates that near infra-red and red edge bands are sensitive to the type of vegetation, the water content, and the tree's health (Chang-Hua et al., 2010, Glass, 2013). The benefit of red edge and near infra-red bands for tree species classification is well explained by Immitzer et al. (2012) in their research on tree species classification of very high spatial resolution. Their research indicates that red and near-infrared reflectance values show higher values for some tree species, as shown in Figures 1-1 below.

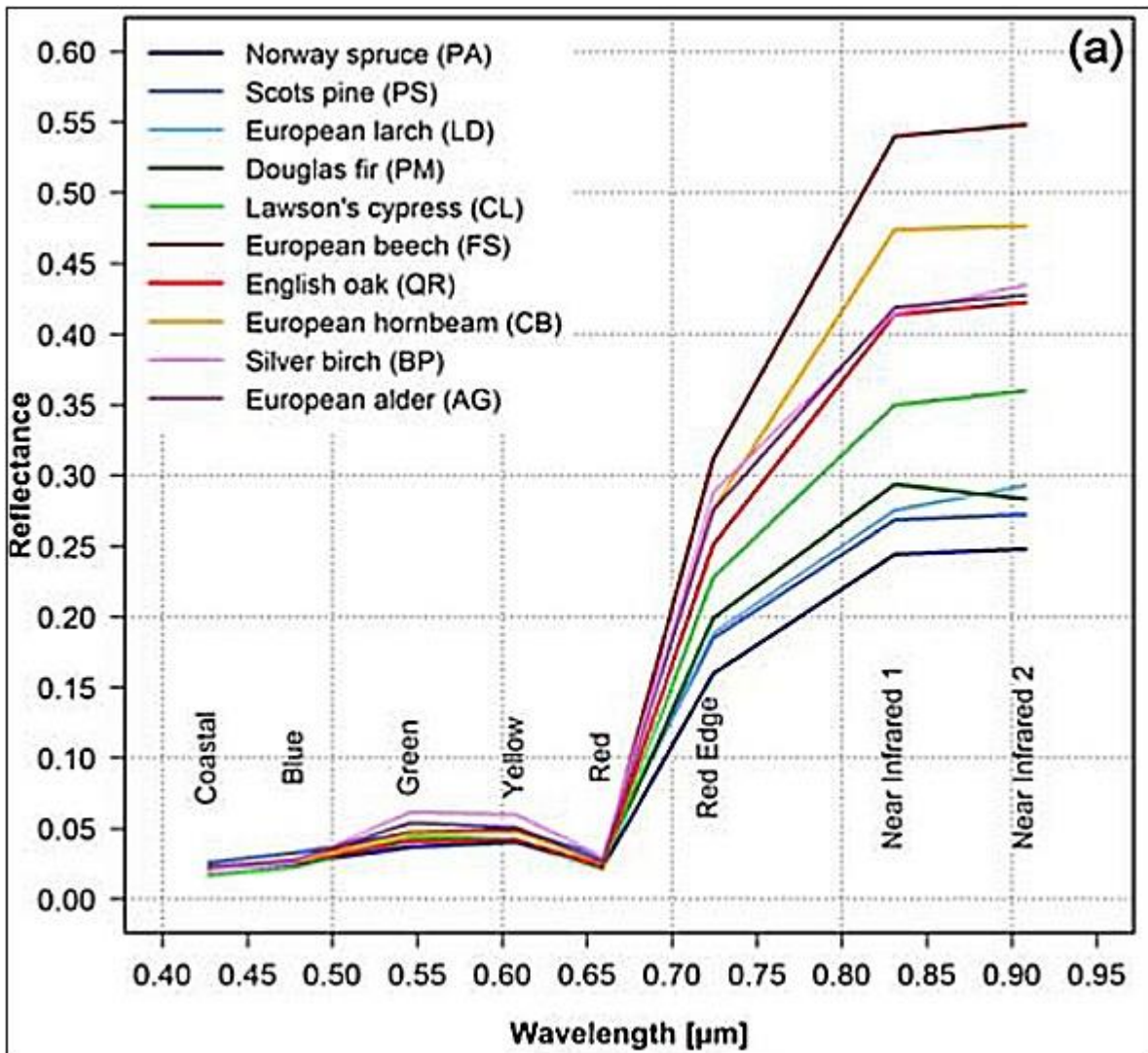


Figure 1-1: Mean spectral signatures of 10 tree species (source: <https://www.mdpi.com/2072-4292/4/9/2661/htm>).

Figure 1-1 above shows that the mean of the spectral signature for ten tree species is close in red, green, blue and coastal, implying low separability for the ten tree species when the red, green, coastal and blue bands are used. However, the near infra-red and red edge bands improve the class separability because the spectral signature is very different which helps separate the tree species and, hence, the tree classification. As the tree goes through the various phenological changes during the seasons, there is spectral variation, and this can also aid in identifying tree species (Sheeren et al., 2016). Natesan et al. (2019) explored the benefit of classifying tree species using three-year multi-temporal UAV-RGB images and reported that using multi-temporal images improves tree species accuracy compared to using a single seasonal UAV-RGB dataset. Their time series analysis for tree species classification resulted in a classification accuracy of 80%. Dymond et al. (2002) and Mickelson et al. (1998) also analysed multi-seasonal Landsat datasets to classify tree species. They concluded that multi-temporal seasonal data yields a better result than using a single season image. The phenological changes of trees captured by remote sensing help identify the tree in different seasons because not all species react the same way and at the same time on different seasons, as shown in Figure 1-2 below.



Figure 1-2: A deciduous tree under different seasons (<https://www.dkfindout.com/us/earth/seasons/four-seasons/>)

From Figure 1-2 above, the tree goes through different phenological changes due to the seasons. The colour of the leaves of deciduous trees changes in fall, and the leaves shed in winter. The leaves grow again in spring, having different colours and in summer become green, unlike evergreen plants that are green through all seasons. These influence the reflectance of the images captured at each season, and this difference when capture can help improve the classification of the tree species. This is especially useful in identifying deciduous trees that change colour and shed their leaves under different seasons. Since the information of the tree is stored during both leaf-on and leaf-off seasons, it helps reduce errors when the tree is identical in a particular season.

Some researchers also utilise textural information to help differentiate between the various tree species. The texture divides images into sections of interest, like species groups, and categorises those sections. Haralick et al. (1973) identified 14 different texture features that are helpful to aid the classification of images. However, Hall-Beyer (2017) identified that while some texture features are helpful in the image classification task, others are not useful as it creates confusion between some classes.

Gray Level Co-occurrence Matrix (GLCM) is a statistical method that can describe the texture properties of an image using the spatial relationship of the pixels (MathWork, 2020). Gray Level Difference Vector (GLDV) evaluates the probability density function for changes observed between image values at positions spaced by pixels and angle (Khazenie & Richardson, 1993). GLCM and GLDV have been used to improve the classification of tree species. Deur et al. (2020) classified tree species in a mixed deciduous forest and used GLCM texture features as input. From the analysis carried out, they concluded that GLCM is the most significant texture feature. Abdollahnejad and Panagiotidis (2020) also classified tree species in a mixed forest and obtained an overall accuracy of 84% using GLDV features as input.

Other researchers utilize image integration to improve tree species classification (Sahu & Parsai, 2012; Ghassemian, 2016). Image integration is a procedure that utilizes the advantage of one dataset to complement the limitation of another dataset to obtain a better result than using a single dataset (Alkema et al., 2013). Sothe et al. (2019) probed the use of hyperspectral images acquired by UAV and photogrammetric point cloud to classify 12 major tree species using support vector machine classifier in a fragmented subtropical forest in Southern Brazil. From their result, using only hyperspectral bands resulted in an overall accuracy of 57% with a kappa index of 0.53. However, including the point cloud dataset resulted in an overall accuracy of 72.4% with a kappa index of 0.70. Nevalainen et al. (2017) also studied UAV-based photogrammetry and hyperspectral performance for individual tree detection and tree species classification in the boreal forest. Their research yielded an overall accuracy of 95% with an F measure of 0.93 when both random forest and multilayer algorithms were used.

Tree species information is valuable to various people involved in forest and tree species management. Accurately estimating all tree species is the desire of all tree species classification tasks, yet this remains a daunting task that depends mainly on the data available, the complexity of tree species present in the study area, and the map's purpose. For instance, a forest manager who wants to know the distribution of tree species and overview the tree species to determine the appropriate silviculture practices to undertake would be interested in obtaining a higher overall accuracy. However, a forest manager interested in identifying timber tree species would want to identify those tree species with higher accuracy than the other tree species present (Duncker et al., 2012). Hence, a compromise must be made to obtain a reasonable overall accuracy for all tree species or high accuracy for some tree species of relevance. This decision depends on the user of the tree species classification map and the purpose of the map.

1.2. Problem statement

Optical remote sensing images provide freely available datasets that can be used to map tree species of both small and large areas. However, cloud cover, spatial and spectral resolution of the satellite image influences the tree species discrimination. UAV has been used to collect cloud-free, high-spatial-resolution images that have improved tree species classification.

Most research uses UAVs to classify tree species, either the red-green-blue (RGB) or multi-spectral bands. Natesan et al. (2019) classified tree species using UAV-RGB images. Their research proposed combining multi-spectral and RGB UAV images for tree species classification to classify tree species such as birch, beech, pine, fir, and spruce. Combining UAV multi-spectral and RGB datasets for tree species mapping is a research area less investigated. Hence, this research was conducted to explore which seasonal dataset is

best for tree species classification and examine the benefit of combining multi-spectral and RGB UAV images for tree species classification.

Forest managers will benefit from such research as it will help them decide when to capture images and which tree species can be identified with such datasets.

1.3. Research objectives

The overall objective of this research is to assess the performance of multi-seasonal UAV-RGB and UAV-multispectral (MSS) images and their combination for tree species discrimination in a mixed temperate forest using a support vector machine classification algorithm.

Specific Objectives:

The specific objectives are:

1. To assess the tree crown delineation accuracy from seasonal UAV-RGB (winter, spring, summer, and autumn) and UAV-MSS (summer) images.
2. To compare the classification accuracy of seasonal UAV-RGB datasets for tree species discrimination in deciduous and coniferous forests.
3. To assess the classification accuracy of the UAV-multispectral dataset for tree species discrimination in deciduous and coniferous forests.
4. To assess the effect of combining summer UAV-RGB and UAV-MSS datasets on the accuracy of tree species discrimination in deciduous and coniferous forests.

1.4. Research questions

- 1a. What are the segmentation accuracies of UAV-RGB seasonal datasets (winter, spring, summer, and autumn)?
- 1a. What is the segmentation accuracy of the UAV-MSS dataset?
2. Which seasonal dataset gives the highest classification accuracy in separating individual tree species in the deciduous and coniferous forest?
3. What is the tree species classification accuracy for UAV-MSS imagery?
4. What is the accuracy of the tree species classification when the summer UAV-MSS and RGB dataset are combined?

1.5. Conceptual diagram

The boundary of the internal system for this research is Haagse Bos in the Netherlands. The sun is part of an external system that emits rays to the forest. While some of the emitted rays are reflected, others are absorbed or transmitted by the atmosphere. The atmospheric conditions determine the seasons that affect the trees' photosynthetic activities, which influences the colour of the leaves.

The transmitted rays from the sun interact with the internal system (forest), which comprises different tree species. This interaction can be detected by the sensors on-board the UAV sensor, and this was analysed during this research to identify the various tree species in Haagse Bos.

Figure 1-3 below shows the interaction between the various system in a conceptual diagram.

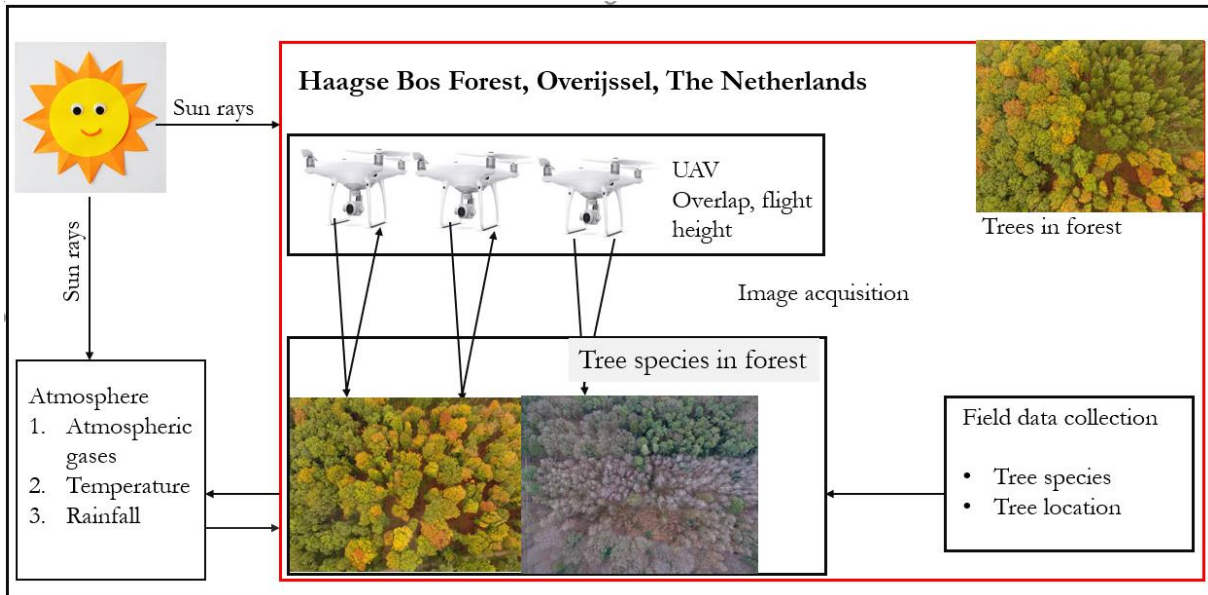


Figure 1-3: Conceptual diagram of system interactions

2. STUDY AREA, MATERIALS, AND METHOD

This section describes the study area for this research, the materials used to gather the relevant information required, and the data processing methods.

2.1. Study area

The study was carried out at Haagse Bos forest, one of the oldest forests in The Netherlands and located in Enschede, Twente Municipality. Haagse Bos forest is about 334 hectares, but the section selected for this analysis is about 43 hectares. It is geographically situated between 476500mN to 477700mN and 261000mE to 262000mE, as shown in Figure 2-1 below.

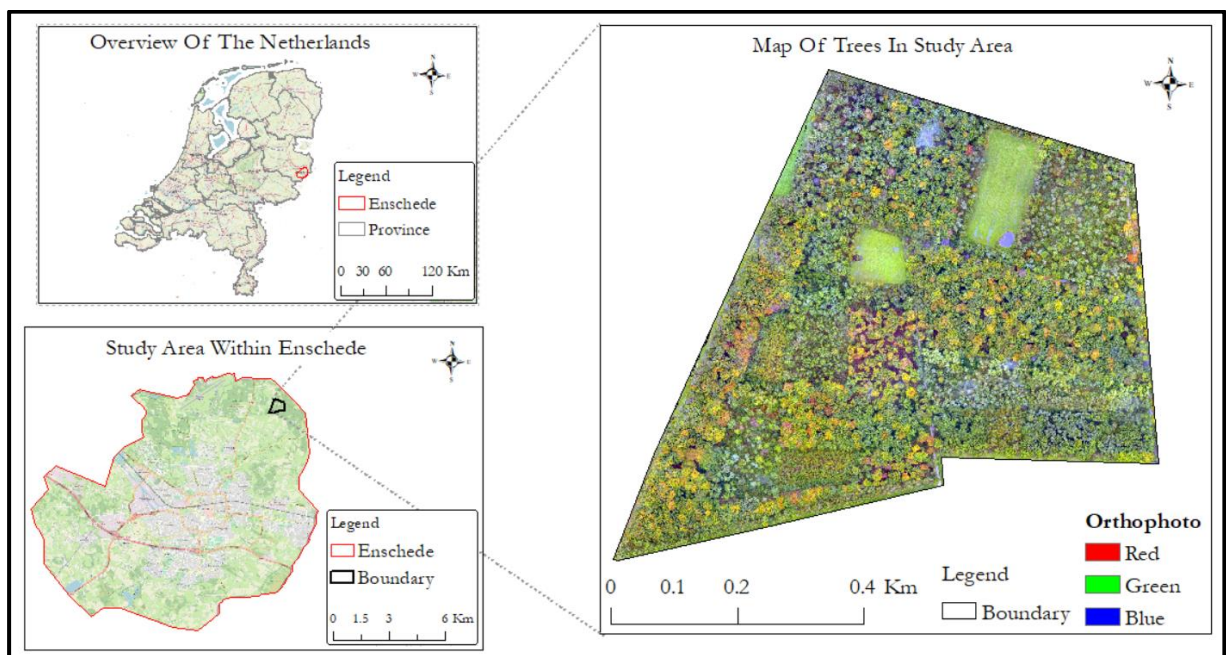


Figure 2-1: Map of the study area, Haagse Bos, Enschede.

This section of the Haagse Bos forest is managed by the NGO “Natuurmonumenten”, which are into nature conservation and recreation. Nature is the habitat of animals and plants; hence, not protecting nature may lead to the extinction of diverse plants and animals in the Netherlands for years (Natuurmonumenten, 2021). Natuurmonumenten protects and preserves the remaining nature and cultural heritage and the future nature area in the Netherlands to protect plants and animals. Natuurmonumenten manages the existing nature conservation that has diverse tree species and plant trees in other areas. Trees are also planted when there is the need to fall a tree due to disease to reduce carbon emissions. Selective thinning is carried out every about every six years. Although thinning is carried out, natural regeneration with human silvicultural activities is part of the Natuurmonumentent management practices (Tenaw, 2011). The study area has broadleaf trees as the dominant tree species.

Haagse Bos comprises young and matured mixed deciduous and coniferous tree species. Typical examples of deciduous and coniferous species to come by in this forest includes Douglas Fir (*Pseudotsuga menziesii*),

Norway spruce (*Picea abies*), Scot pine (*Pinus sylvestris*), European Larch (*Larix decidua*), Oak (*Quercus robur*), European white birch (*Betula pendula*), European beech (*Fagus sylvatic*), and Alder (*Alnus glutinosa*).

The terrain is relatively flat with a mean annual rainfall of 841mm, mean annual minimum and maximum temperature of 6.6°C and 13.5°C. The month of November records the highest rainfall in the year. The coldest and warmest months in the year are usually January and August, respectively.

Haagse Bos was chosen for this study because it was possible to fly the UAV for data collection, although there are restrictions for flying the UAV in the Netherlands. Also, the Haagse Bos forest had a good composition of different tree species and was easily reachable for fieldwork due to its proximity to the University of Twente.

2.2. Material

Different types of equipment were used for the data collection. Table 2-1 below shows the equipment that was used to acquire the data needed for this research.

Table 2-1: Field instruments and their use on the field.

Instrument	Use
Ground Control point (GCP) markers	To establish temporary GCP
Differential Global Navigational Satellite Systems (DGNSS) Real-Time Kinematics (RTK)	For measuring coordinates of GCPs
Tablet/Mobile phone	For navigation and data collection
DJI Phantom 4 Pro	For acquiring the UAV-RGB images
Sequoia multi-spectral sensor	For acquiring the multi-spectral images

UAV data and tree species information were collected and used for further analysis to answer the research questions. The fieldwork was carried out between August and October 2020. The software for data collection and processing are shown in 2-2 below.

Table 2-2: Software and its uses

Software	Use
Pix4D Capture	UAV flight planning
Avenza mobile app	For navigation and capture of tree species information
DJI 4 Go	UAV configuration
yED Graph Editor	Flowchart
Pix4Dmapper 4.6	Processing UAV images
eCognition Developer 10.0	Image segmentation, classification, and accuracy assessment
Google Earth Pro	Extracting coordinate (e.g., location of GCP)
ArcMap 10.8	Preparing maps
Python (Scikit learn)	Parameter tuning for image classification
Microsoft word	For report writing
Microsoft excel	Making graphs
Mendeley Desktop	Referencing

2.3. Method

The method deployed in this study involves four main steps. Step 1 was a reconnaissance survey and field data gathering which includes observing and identifying tree species present. Also, the optimal location to place the ground control points was identified. Step 2 was processing the UAV data that was acquired to obtain the UAV outputs (orthophoto, DSM, and DTM). The DSM and DTM were used to estimate the canopy height model (CHM), which was also used as input in the machine learning classification algorithm. The image segmentation was carried out to determine the tree crown in Step 3. Finally, step 4 involves image classification using machine learning and estimation of accuracy of the classified tree species. Figure 2-2 below shows the flowchart of the method used.

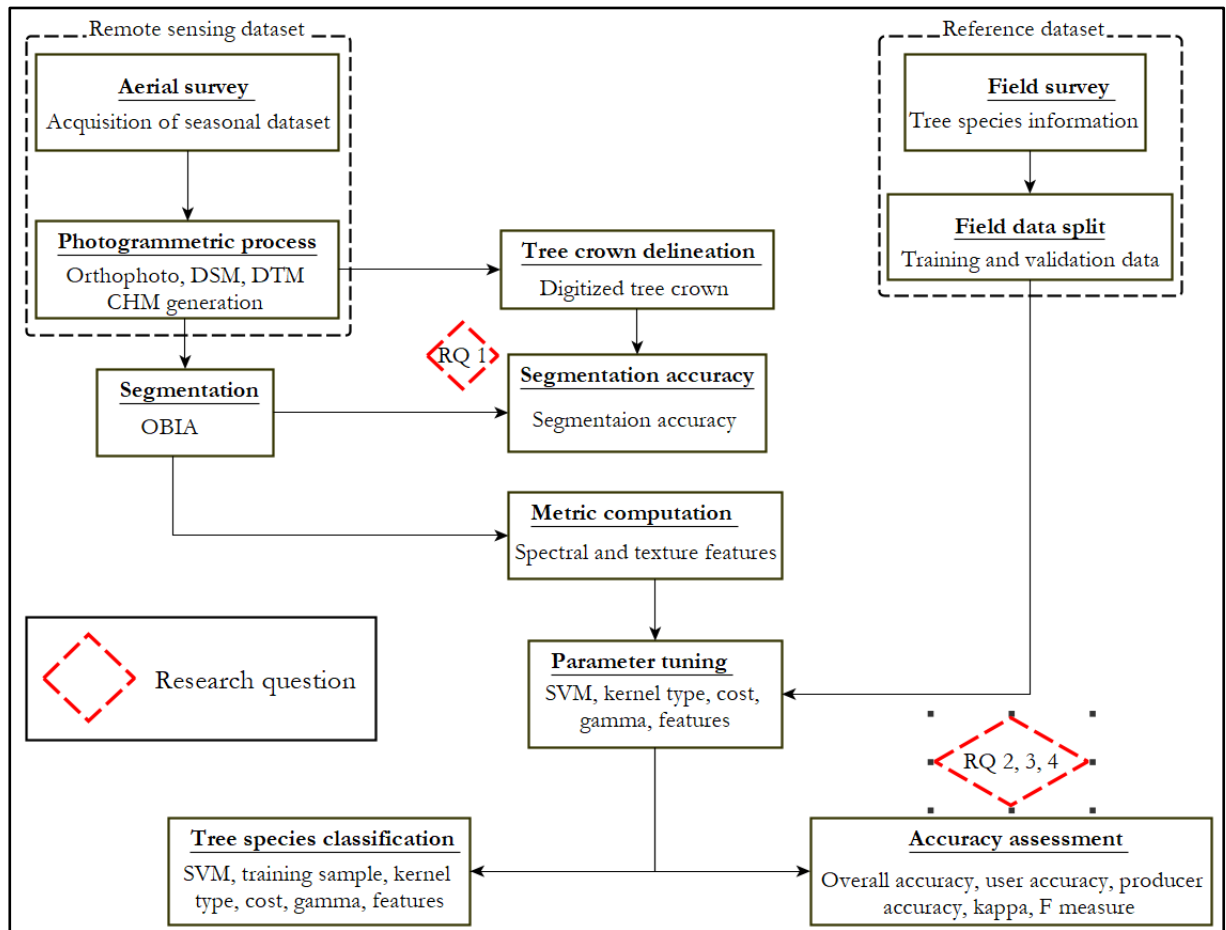


Figure 2-2: Flowchart of method

2.4. Fieldwork

2.4.1. Pre-fieldwork desk study

Before the data collection, an overview of the study area was observed on Google Earth Pro. Using Google Earth Pro, the open area to place the temporary GCPs was identified, and the coordinates were recorded on an android phone using the Avenza app. A visual inspection was used to identify some tree species in the study area, and the data were compared with the information collected by Eshetae (2020).

After obtaining the relevant information during the pre-fieldwork desk study, the fieldwork was carried out.

2.4.2. Reconnaissance survey

The reconnaissance survey was carried out during the fieldwork to verify the information obtained during the desk study. For instance, the location of the GCPs identified during the desk study was confirmed. Also, the tree species identified were verified, and some corrections were made to improve the data obtained during the desk study.

It appeared that some tree species were few in numbers (such as red beech, chestnut, etc.), where others were many. In addition, broadleaved trees are the dominant tree species compared to coniferous tree species. The reconnaissance survey helped to obtain a broader perspective of the study area. After the reconnaissance survey, I planned the sampling design for data collection.

2.4.3. Sampling design

A purposive sampling scheme was used to collect the field data. A purposive sampling scheme is a sampling scheme that is based on the researcher's judgment. The purposive sampling method was used because of prior knowledge of the study area. Purposive sampling enables enough data to be collected in less time.

2.4.4. UAV data acquisition

UAV has gained popularity for data collection due to obtaining high spatial and temporal resolution images (Yao et al., 2019). The UAV-RGB and multi-spectral datasets were the two different data types used for this research. The UAV-RGB and MSS sensors were used to collect the summer dataset.

DJI Phantom 4 Pro drone with RGB and Sequoia cameras was used for the data collection. Figure 2-3 below shows the UAV with RGB and Sequoia camera and AIRINOV target for data collection.



Figure 2-3: Sequoia camera mounted on DJI Phantom 4 Pro and AIRINOV target

Figure 2-3 above shows that the DJI Phantom 4 Pro UAV was modified to hold the multi-spectral Sequoia camera during the data acquisition. The Sequoia camera is a multi-spectral camera used to obtain data in the green, red, red-edge, and near infra-red bands compared to the regular Phantom 4 Pro camera used to get information red-green-blue (visible) bands. Also, the Sequoia camera has a 16-bit megapixel RGB camera enabling it to store an extensive range of values that can help distinguish features compared to the DJI Phantom 4 Pro, which has an 8-bit megapixel (senseFly, 2021). The AIRINOV target was used for the radiometric calibration of the Sequoia sensor before and after acquisition of the MSS dataset.

The GCPs were then placed at the optimal location identified during the pre-fieldwork and verified during the reconnaissance survey. Fourteen GCPs were distributed over the study area to be used to orient the acquired UAV images. Figure 2-4 below is a sample of the GCP.



Figure 2-4: Recording 3-D coordinate of GCP with DGNS RTK in an open space

The three-dimensional (3-D) coordinate of the GCP placed in an open area, as shown in Figure 2-4 above, is collected using a DGNS RTK instrument.

Before the commencement of the flight, the compass was tuned, and the home location of the UAV was set using DJI Go 4 software. The quality of UAV output generated is dependent on the point clouds generated, which is obtained when using high forward and side overlaps, although this increases the data acquisition time (Obeng-Manu, 2019). Large forward and side overlaps were used to get quality UAV output for the analysis, as shown in Table 2-3 below.

Table 2-3: UAV flight plan

UAV flight Parameters	Value
Flight Pattern	Double grid
Camera angle	90 degrees
Speed	Slow
Front Overlap	90%
Side Overlap	80%
Flight Height	120 m
Resolution	4.6 cm/pixel

With the flight plan above and GCP placed at the appropriate location, the UAV images were acquired with RGB and sequoia multi-spectral cameras.

The summer UAV-RGB and UAV-MSS datasets were acquired on 4th August 2020. Dataset for September 2019, February 2020, and May 2020 were available from the previous studies carried out by Eshetae (2020), Gaden (2020), Bediako (2020) and this data was collected with the RGB sensor. The details of UAV images of earlier seasons are shown in Table 2-4 below.

Table 2-4: Data from previous studies

Season	Data type	Resolution	Date capture
Fall	UAV-RGB images and GCP coordinates	4.6 cm/pixel	12 th October 2019

Winter	UAV-RGB images and GCP coordinates	4.9 cm/pixel	14 th February 2020
Spring	UAV-RGB images and GCP coordinates	4.58 cm/pixel	15 th May 2020

To guarantee all datasets were consistent and to enable comparison to be carried out for the different seasons and datasets, the same flight parameters (flight height and overlaps) as those used by previous studies. The output of the UAV data was used as input for the tree species mapping.

2.4.5. Tree species identification

The UAV images collected during the UAV image acquisition were processed using Pix4DMapper to obtain the orthophoto, DSM, and DTM. The orthophoto was uploaded into the Avenza mobile app for collecting the tree species data. Due to the error inherent in mobile phone GPS, the map was printed on A3 paper and laminated to identify the tree species in the field.

The study area has homogeneous parts with clusters of similar tree species, while other regions had a mixture of tree species. A minimum of two field points were generated for each tree species class, and plots with a radius of 12.62 m per field point were established. The tree species within the sampling radius that were identified on both the printed orthophoto and the field were recorded. A total of 238 trees species information was collected.

In addition, 500 random points were created using ArcMap in the areas with homogenous and mixed species. This was done to increase the number of samples as some tree species were underrepresented with less than 30 trees. The random points that intersect with the trees that were already recorded in the sampling radius were deleted to avoid double counting of the same tree. Out of the 500 random points generated, 186 were used to collect tree species information.

Some non-tree species data were gathered to aid the classification. Water, grass, bare ground (soil) and undergrowth were merged and labelled as non-tree. A total of 87 non-tree samples were collected.

Some tree species information from previous studies carried out at the same study area was also available. To obtain a good distribution of the field data, 132 tree species information available from previous studies was added. A total of 643 field points were used for the analysis, as shown in Table 2-5 below.

Table 2-5: Tree species and samples collected.

Category	Tree species	Scientific name	Sample collected
Broadleaved	European white birch	<i>Betula pendula</i>	60
	European red beech	<i>Fagus sylvatica</i>	14
	European beech	<i>Fagus sylvatic</i>	90
	Chestnut	<i>Castanea sativa</i>	8
	Mountain ash	<i>Sorbus aucuparia</i>	8
	Oak	<i>Quercus robur</i>	97
Coniferous	Scot pine	<i>Pinus sylvestris</i>	59
	European larch	<i>Larix decidua</i>	50
	Douglas fir	<i>Pseudotsuga menziesii</i>	86
	Norway Spruce	<i>Picea abies</i>	84
Non-tree	-	-	87
Total			643

The tree species information was acquired between 5th and 23rd October 2020

2.5. Data processing

The data processing was carried out in four different phases, namely:

- Structure from Motion (SfM): to obtain the orthophoto, DTM, and DSM from the UAV images
- Object-Based Image Analysis (OBIA): to get the tree crowns from the object segments created from the image segmentation process.
- Tree species classification: the pre-processing and classification of input data to obtain the classified tree species.
- Accuracy assessment and statistical analysis: to analyse the result from the tree species classification.

2.5.1. UAV-RGB image processing

The 2-D UAV images obtained during the UAV flight can be processed using structure from motion (SfM) technique to 3-D information (Alcantarilla et al., 2012). SfM is possible due to advance made in computer visions couple with photogrammetric workflow (Kachamba et al., 2016). The 3-D information are extracted by identifying the same features on the overlapping images through stereo vision (Nex & Remondino, 2014). For the successful implementation of SfM to identify the features of interest, the images must have overlaps and be captured at different location as shown in Figure 2-5 below.

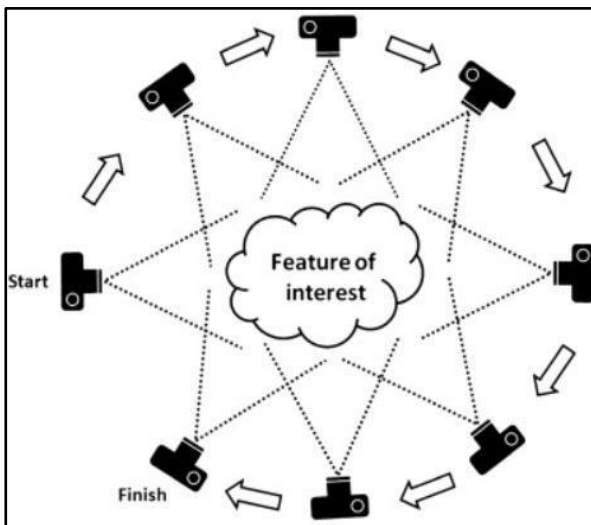


Figure 2-5: Overlapping images observing the same features at different location (Westoby et al., 2012).

The features of interest, shown in Figure 2 above, are first identified, traced and matched from one image to the other to compute their position using Random Sample Consensus (RANSAC) algorithm (Fischler & Bolles, 1987). The features of interest identified are termed as tie points and these are used to estimate the initial position of the camera, scene geometry, and the coordinate of the feature (Westoby et al., 2012). The number and quality of the tie point generated are dependent on the image resolution, number of overlapping images used, and setting used when processing the data (Pix4D, 2021). The initial results are iteratively improved using least square minimization (Snavely et al., 2008). The initial results obtained are in a relative coordinate system, hence has no scale and orientation in relation to the real world. The initial results are converted from relative image space to coordinate system on ground using ground control points through Bundle Block Adjustment (BBA) (Westoby et al., 2012). The BBA is also used to evaluate the geo-refencing error and decrease the variation between the observed and predicted image locations using a non-linear least square approach (Nex & Remondino, 2014). The generated point clouds are classified into points on ground and other points. The points on ground are used to determine the DTM using an interpolation algorithm while all the points generated are used to generate the DSM. The DSM and image block generated are used in an orthorectification process to generate the orthophoto (Nex & Remondino, 2014). According to ESRI (2016), the orthorectification process involves eliminating relief effect from an image.

The acquired UAV images (four RGB and one MSS) were processed using Pix4D mapper software, which works by incorporating the SfM algorithm (Pix4D S.A., 2017). This was carried out in three main steps:

- Initial processing: the tie points (referred as key points in Pix4D) were detected and matched from one image to the other. The camera calibration and point cloud densification were automatically executed through the Automatic Aerial Triangulation. The BBA was then used to geo-reference the dataset using the GCPs loaded and the control points (CP) used to calculate the georeferencing error (Pix4D, 2020). A quality report generated is used to determine if the georeferencing error is acceptable before the next phase of the analysis.
- Point cloud and mesh: this phase increases the density of the 3D points generated at the initial processing step to increase the accuracy of DSM, DTM, and orthophoto that will be generated in the next phase. The point cloud densification image scale was set to full to utilize the original image size. This increases the processing time but yields better results. The point density was set to optimal and minimum number of matches set to 7.
- DSM, DTM and orthophoto: the dense point clouds generated were used for the generation of DTM, DEM, and orthophoto. The automatic resolution of 1 GSD was selected, noise filtering and use surface smoothing for the DSM selected. The inverse distance weighting algorithm was selected for the DSM generation and the merge tile selected for both the DSM and orthophoto.

The process was repeated for all seasonal UAV-RGB. The RMSE was 0.005 m for the fall dataset, 0.08 for the summer dataset, 0.02 for the winter dataset, and 0.04 for the spring dataset. The UAV orthophoto per seasonal dataset is shown in Figure 2-6 below.

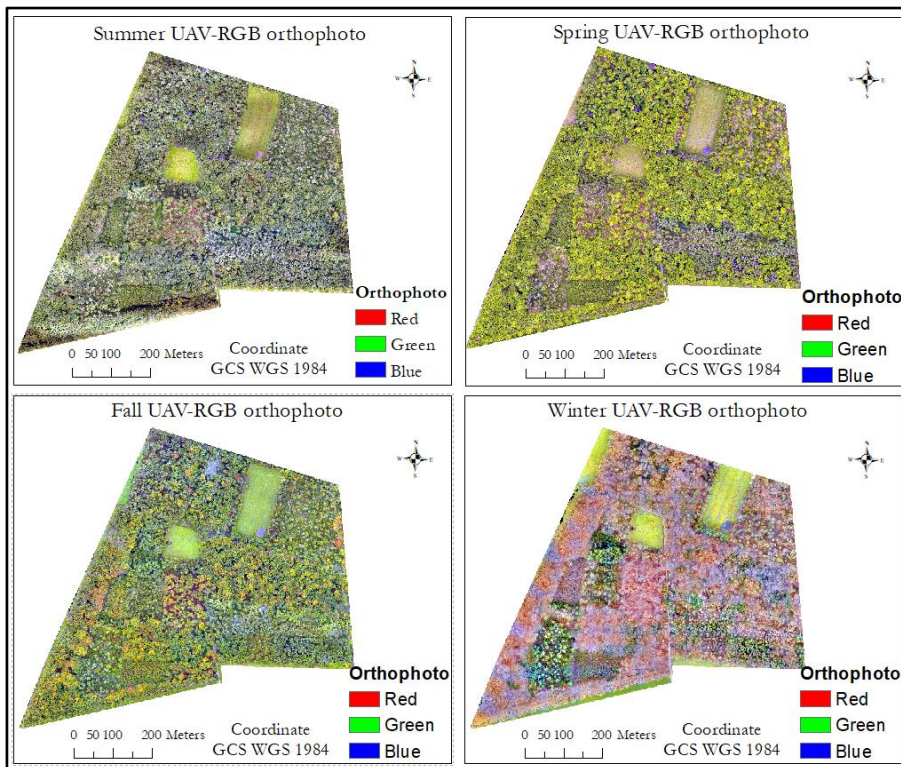


Figure 2-6: Orthophoto of the summer, spring, fall, and winter dataset.

2.5.2. UAV-MSS image processing

A project was created for the UAV-MSS data processing in Pix4D and all the images, including the image of the calibrated targets. Coordinate of the images were then selected. The ‘Ag multispectral’ template was chosen for the processing. The Index calculator in the processing option was checked to make sure the radiometric calibration target data was automatically detected for all the multispectral bands, then finally, the process was started. The workflow for UAV-RGB was repeated for the MSS using the MSS settings stated above. The georeferencing error was 0.059m for the UAV-MSS dataset. Figure 2-7 below shows the output of the UAV-MSS processing.

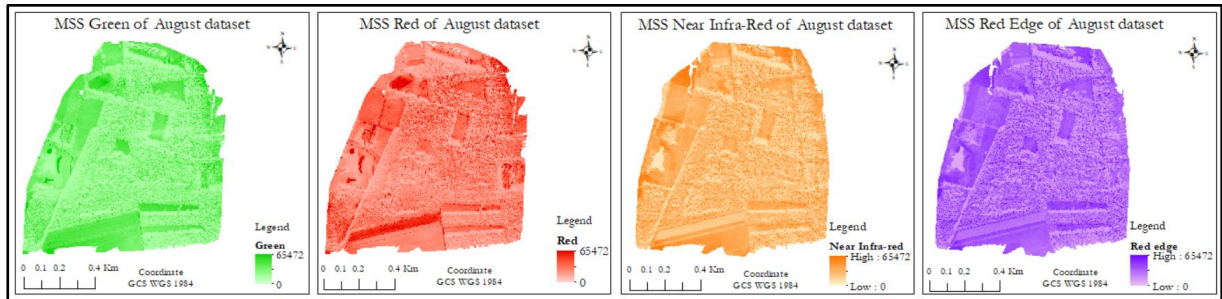


Figure 2-7: Green, red, near infra-red, and red edge bands from the summer MSS dataset.

2.6. Data analysis

2.6.1. Pre-processing

The same flight parameters used during the previous study were used during the image acquisition. However, the images had slightly different spatial resolutions. To obtain similar image resolution, all the orthophoto datasets were filtered with a 3*3 low pass filter to remove eliminate noise and tiny image objects that may be created during the segmentation process (Kejriwal & Singh, 2016; Gao et al., 2017). The orthophotos were then resampled to 10 cm using the nearest neighbour algorithm to conserve the spectral properties of the pixels. 10 cm was chosen for the resampling because the study comprised of both young and mature forests

2.6.2. Image segmentation

Object-based image analysis (OBIA) is a procedure that extracts image object from an image. The recent availability of very high-resolution images which contain more information that cannot be adequately processed with pixel-based analysis brought a shift in image analysis, from pixel-based to object-based (Zhu et al., 2016; Wang et al., 2018).

The input dataset was loaded into eCognition software. The normalised Digital Surface Model (nDSM) layer calculation algorithm created the canopy height model (CHM) for all the seasons before initiating the OBIA. The nDSM algorithm determines the arithmetic difference between the DSM and DTM. The nDSM output is an essential layer that aid to discriminate between elevated and non-elevated datasets, which can be used to improve the classification (eCognition, 2020). Figure 2-8 above shows the CHM for the UAV-RGB dataset.

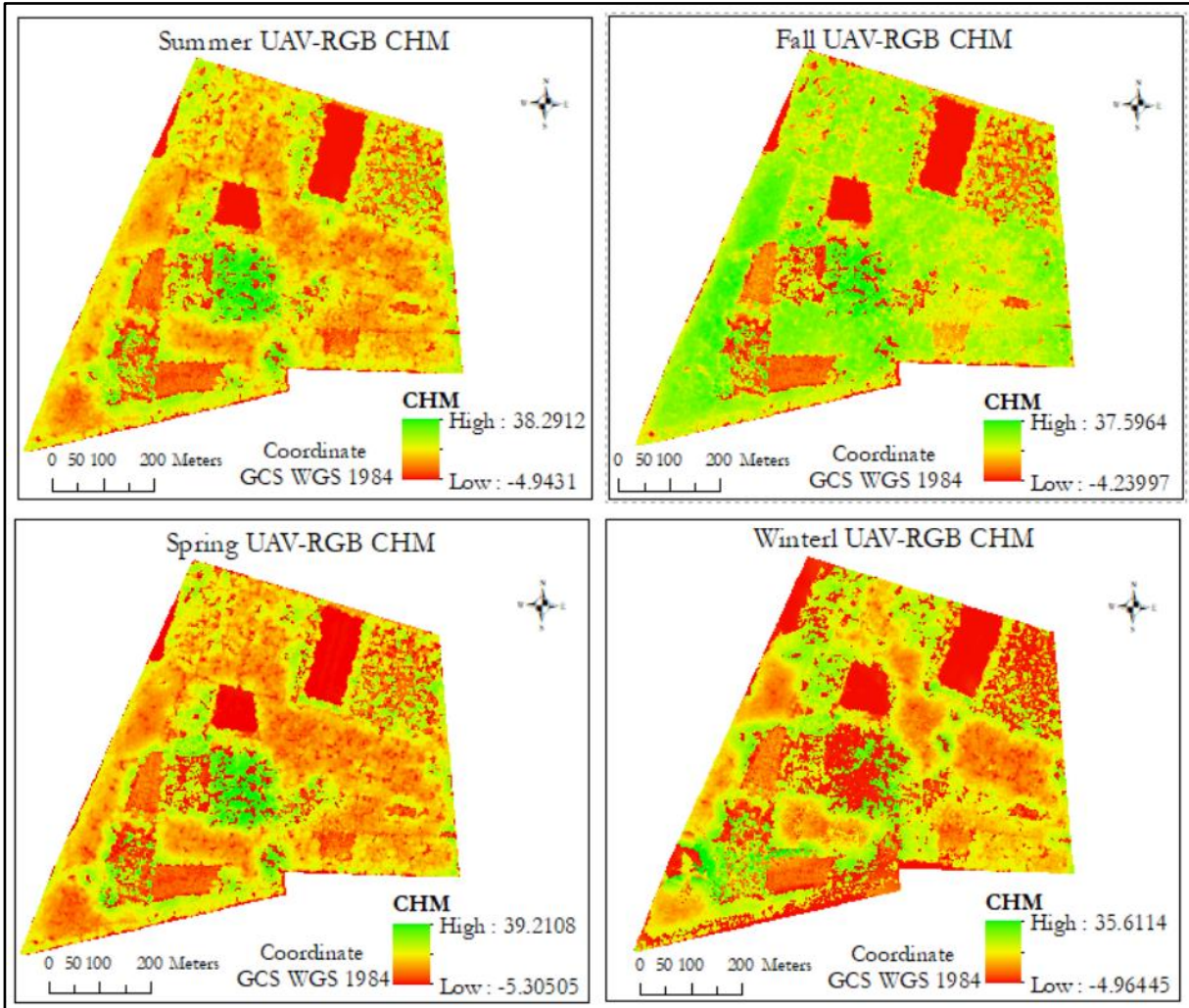


Figure 2-8: CHM of the summer, spring, fall, and winter dataset.

Image segmentation is the primary step when carrying out OBIA. The multi-resolution segmentation (MRS) algorithm was used to obtain homogenous objects because the algorithm decreases the object heterogeneity while exploiting the object homogeneity as tree crowns are homogenous compared to the surrounding shadows and undergrowth (Baatz & Schäpe, 2000). The MRS is a bottom-up merger method that iteratively grows by combining the small segments into a bigger segment until the homogenous threshold of the image object is achieved or exceeded. This homogenous threshold is part of the input parameters (such as scale, shape, compactness, image layer) that the user decides. Below is the significance of the parameters used:

- The scale parameter is a parameter that defines the maximum heterogeneous image segment that can be obtained. Scale is the parameter that directly controls the size of the image objects (tree crown). When the scale parameter is large, a large image object with high heterogeneity is produced and vice versa.
- Compactness indicates the compactness of the image objects. A high compactness value results in creating compact image objects.
- The shape parameter helps to include the influence of spectral values on the heterogeneity of the segment created. Reducing the shape creates image segments that have less spatial homogeneity and heterogeneity.
- Image layer weight determines the influence of the input layer band on the segmentation process (Landmap, 2021).

Although the relevance of the parameters is known, identifying the optimal parameters requires a lot of experimentation which is time-consuming. The Estimator Scale Parameter (ESP) tool was used to determine the optimal scale parameter to generate the image segments. It allows the user to define the step size, which controls how the segmentation parameters are increased (Drăguț et al., 2014). The ESP tool creates image objects into three levels (i.e., from finer segments to courser segments) to calculate the local variance of the image objects. The output of the ESP analysis is shown in Figure 2-9 below.

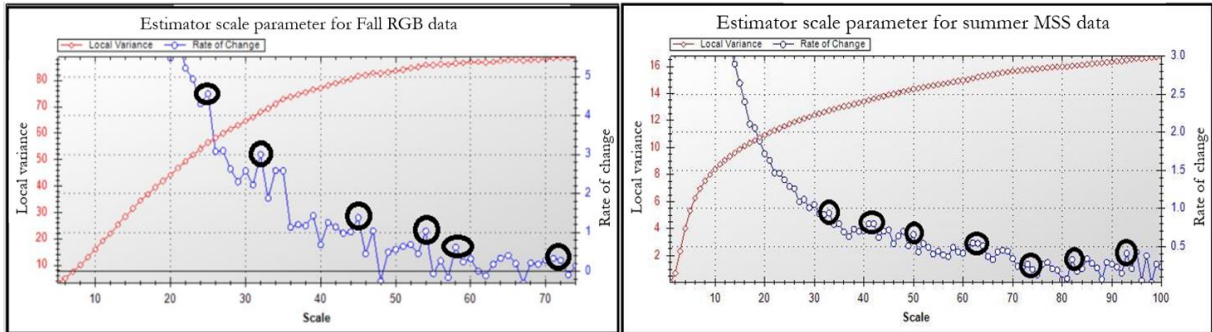


Figure 2-9: ESP result for fall RGB and summer MSS dataset.

From Figure 2-9 above, the black circles are the scale parameters identified when the ESP plugin was used to identify the parameters for the image segmentation. The scale parameters of 24, 32, 44, 55, 57, and 72 for Summer RGB dataset (shown in Figure 3-2a) and 32, 43, 50, 62, 74, 83, and 93 (shown in Figure 3-2b) for the Summer MSS dataset. These selected scale parameters were used for different segmentation tests in eCognition. These scale parameters were chosen because of the rate of change curve, as they represent the highest peaks. The high peaks indicate the scale parameters at which the resulting image objects depict a homogenous image segment. Figure 3.2 describes the variations in local variance shown in the red curve and the rate of change with increasing scale parameter, shown in the blue line. These selected scale parameters were used for image segmentation and the procedure repeated for the other datasets. The scale parameters that yielded the best segmentation accuracy were selected as the optimal scale parameter from the test. The optimal scale parameters were 72 for the summer RGB image, 64 for the fall RGB image, 54 for the spring RGB, 37 for the winter RGB, and 74 for summer MSS images. The scale parameters such as 24, 32, 43, 44, 50, 55, 57, and 62 resulted in a lot of under-segmentation while 83 and 93 resulted in over-segmentation.

After identifying the optimal parameter for the segmentation, the MRS was used to generate the segment, and the result is shown in Figure 2-10 below.

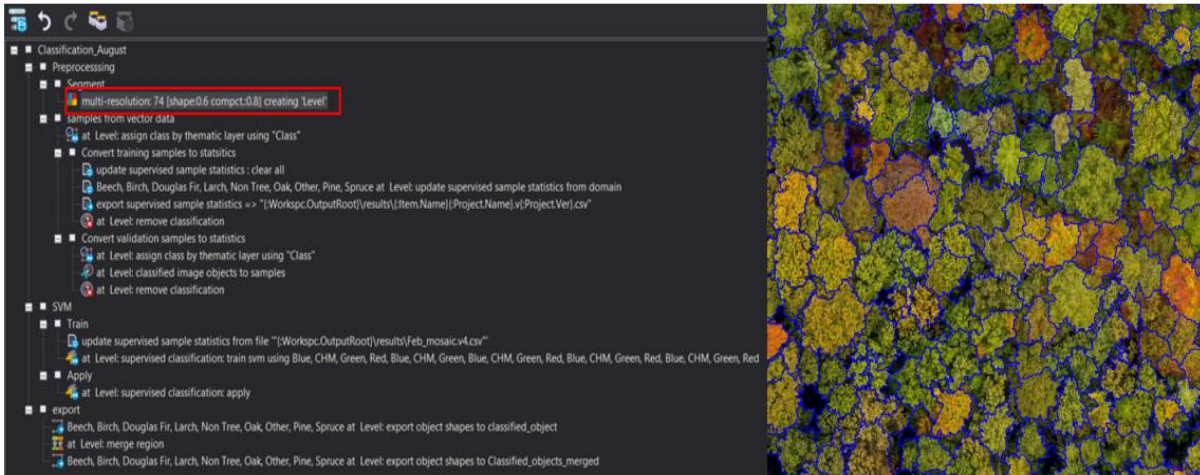


Figure 2-10: Ruleset for segmentation (in red) and classification with the resulting segment.

Figure 2-10 above shows the ruleset used and the image segment created for the fall RGB dataset. A ruleset is a group of individual processes used to carry out a specific task (eCognition, 2019). The image segment created from the MRS is shown in blue colour.

2.6.3. Manual digitising of tree crown

The manual digitising of individual tree crowns was performed after obtaining the output from the UAV data processing. The digitising was carried out on the resampled images. The manually digitised tree crown was used as a reference to determine the segmentation accuracy by comparing it to the image segment created.

The input for the digitising was the canopy height model and orthophoto. The crowns of tree species that were identified on the orthophoto were digitised using ArcMap. However, tree crowns that were difficult to determine mainly due to the combination of tree crowns were identified using the swipe tool to view the CHM and orthophoto simultaneously. Also, the individual UAV images aided in the manual delineation. Figure 2-11 below shows a section of the manually digitised image objects.

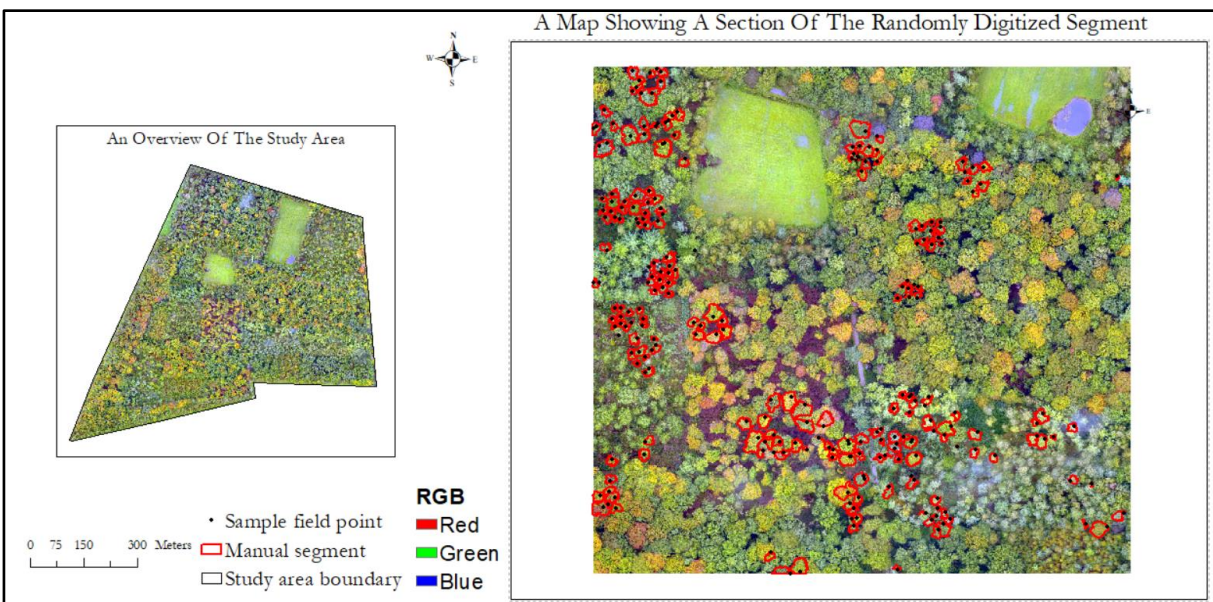


Figure 2-11: A mapping showing the manually digitised segments

Figure 2-11 above shows the result of manually segmenting about 150 segments for segmentation accuracy.

2.6.4. Segmentation accuracy

The segments created during the image segmentation process were assessed to determine how the segments fit the tree crown. This is essential because the segment represents the tree crown; hence it is vital to get the tree crown as accurately as possible to improve the classification.

The accuracy assessment of image objects was carried out using the area estimation approach proposed by Clinton et al. (2010). This approach is based on equations 1-3 below.

$$\text{over segemation}(X) = 1 - \left(\frac{\text{area}(ASI \cap AMP)}{\text{area}(ASI)} \right) \text{-----} \text{eq1}$$

$$\text{under segemation}(Y) = 1 - \left(\frac{\text{area}(ASI \cap AMP)}{\text{area}(AMP)} \right) \text{-----} \text{eq2}$$

$$\text{Total detection Error}(\text{segemation error}) = \sqrt{\frac{(X^2 + Y^2)}{2}} \text{-----} \text{eq3}$$

Where;

ASI is an area of the segmented object by multi-resolution segmentation algorithms (MRS)

AMP: area of the reference polygon (tree crown) which is manually digitized in ArcGIS

Area (ASI ∩ AMP): area of manually delineated polygon correctly identified by MRS

The error is determined by estimating the mean of over-segmentation and under-segmentation. After evaluating the error, the accuracy was determined using equation four below.

$$\text{Segmentation accuracy} = 1 - \text{Total detection Error (segmentation error)} \text{-----} \text{eq4}$$

2.6.5. Field data split

The tree species information captured on the field was exported to excel. The classification task required numerical data as input; hence the exported tree species information was recorded as shown in Appendix 1.

The tree species with samples less than 30 were grouped and classified as other species. Thirty was chosen as the threshold because that is the minimum sample required for the sample to be normally distributed.

The recorded field data was then imported to python. The train test split function in the Scikit-learn package was used to split the field data. Seventy percent of the data was used for training and thirty percent for validation. The training and validation excel sheet was then converted to shapefile to be used in eCognition classification.

2.6.6. Feature extraction

Features that have information to separate one tree species from the other are essential when classifying image objects using machine learning. A mixture of spectral and textural features was extracted using eCognition because research has identified that multiple features based on predefined selection criteria may improve classification accuracy (Xie et al., 2019; Cao et al., 2018). While some research reported that GLCM helps improve classification (Deur et al., 2020), others reported that GLCM does not improve tree species classification (Yang et al., 2019). All the spectral and texture information available in eCognition was utilised to determine if it can enhance the tree species classification is shown Appendix 2.

The texture features available on eCognition are (Mryka Hall-Beyer, 2017):

- The angular second moment is also referred to as energy. It provides the sum of squared elements in the statistical method used. A high angular second moment implies the pixels are similar and homogenous.
- Contrast: indicates the local variation existing in an image.
- Correlation: indicates the linearity of the image. A high correlation indicates a high amount of linear structure.
- Dissimilarity: indicates the local intensity variation defined as the mean of the absolute difference between the neighbourhood pairs.
- Entropy: is a measure of the information content. It indicates the randomness or homogeneity of the image intensity.
- Mean: refers to the mean of the pixel values in a window.
- Standard deviation: refers to the standard deviation of the pixels in a window.
- Homogeneity: indicates the uniformity of elements in the image.

The above texture information can be extracted using many statistical approaches. Gray Level Co-Occurrence Matrix (GLCM) and Gray Level Difference Vector (GLDV) are the two statistical approaches used to estimate the texture features by considering the spatial relationship of the pixels. GLCM calculates texture properties by determining how often pixel pairs with specific values and a specific spatial relationship occurs in an image (MathWorks, 2020). GLDV is used to determine the probability density function for discrepancies between image function values at locations spaced d pixels apart and at an angle.

All the spectral and textural features available in eCognition were exported for further analysis as shown in Appendix 2. Features with high correlation were dropped because features with high correlation have similar information. This reduces the processing time. The remaining features were used in a parameter tuning test to identify the best features that improve the tree species classification for the seasonal RGB, summer MSS and combination of summer MSS and RGB datasets.

The combination of RGB and MSS datasets was achieved by appending the blue band from the RGB dataset to the MSS bands. Although both MSS and RGB datasets have red and green bands, the data range for the MSS dataset enables it to improve class separability. Hence the red and green bands from MSS was used.

To identify the optimal parameters for the classification, the training and validation dataset was loaded into the project created for each seasonal dataset in eCognition. The assigned class by thematic layer algorithm was used to allocate image objects to the training/validation samples. In so doing, the training/validation data, which is point data, is converted to the corresponding image object that overlaps spatially. The updated supervised sample statistics algorithm was used to append all the features per dataset. The result was converted and exported to CSV using export supervised sample statistics.

The features that were identified per seasonal dataset to be used for the classification is presented in Appendix 3. Figure 2-12 below shows the summer RGB feature used for the tree species classification.

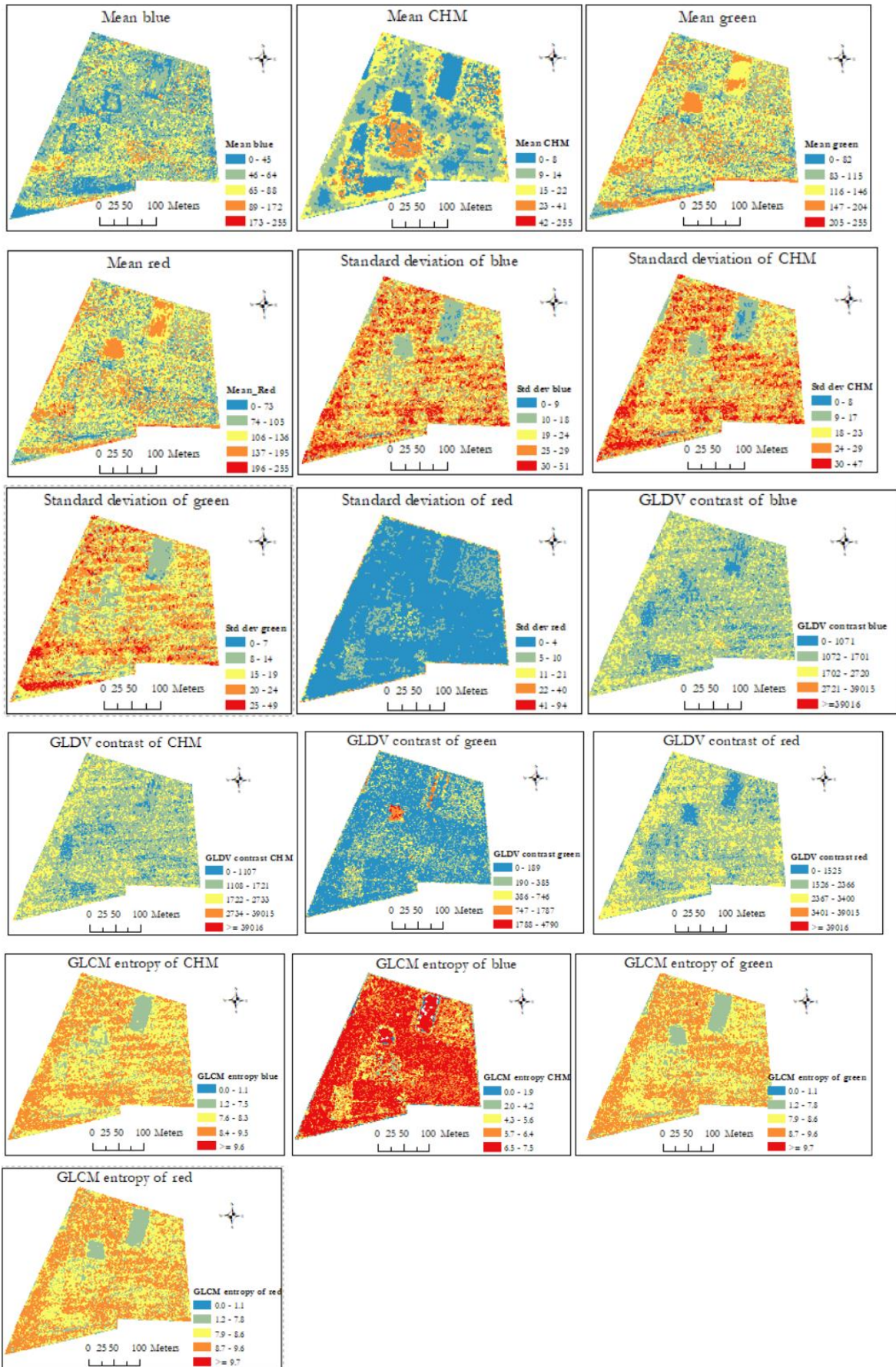


Figure 2-12: Features for summer UAV-RGB dataset classification

From Table 2-7 above, different features are used for different seasons. Different features are used for each seasonal dataset because each seasonal dataset has different spectral and spectral properties per tree type. Hence, the features that can help identify trees in summer may not identify tree species in winter or fall.

It is also possible to use vegetation indices as input during the tree species classification. Vegetation indices are sensitive to the tree's chlorophyll content and have been used as input for the classification task. However, these indices cannot be estimated using the UAV-RGB dataset because that sensor can only provide information about red, green, and blue bands and not red-edge and near infra-red, which are usually required to estimate vegetation indices. The multi-spectral dataset, on the other hand, has the red-edge and near infra-red band. The MSS dataset was obtained in summer, and in summer, the trees, undergrowth, and grass are green. Observing some vegetation indices (normalised difference vegetation indices and difference vegetation index) for some tree species and non-tree species (undergrowth and grass) showed little or no variation.

2.6.7. Tree species classification

According to Duque et al. (2017), classification can determine the relationship between a set of categorical variables using quantitative methods. Classification can be carried out using either the traditional approach or machine learning. Advances made in machine learning make it possible to extract hidden information in the data, improving the classification result (Carrio et al., 2017).

Support Vector Machine classification (SVM) algorithm was used to classify the tree species because research has found that it results in higher classification accuracy compared to maximum likelihood classifier. It can be used for complex modelling and modelling of high dimensional feature spaces (Heumann, 2011; Xie et al., 2019). Also Eshetae (2020), who carried out tree species classification research on the same study area, recommended that an SVM classifier be used to classify UAV data in Haagse Bos as it yields higher classification accuracy than the decision tree and random forest algorithms. The SVM classification algorithm separates the number of classes by finding the best hyperplane using support vectors from data points obtained from the training dataset (Xie et al., 2019) as shown in Figure 2-13 below.

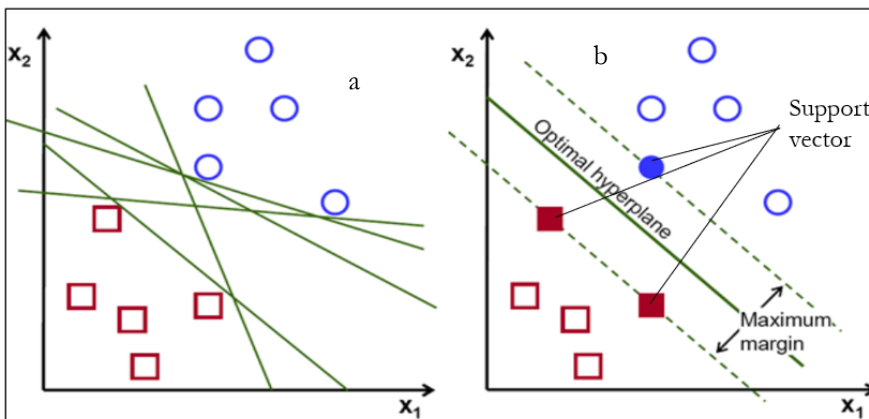


Figure 2-13: Possible planes that can separate classes (a) and optimal plane that can separate classes (source: <https://towardsdatascience.com/svm-feature-selection-and-kernels-840781cc1a6c>)

Figure 2-13 above shows two graphs; graph a shows two classes (one in blue circle and the other in red square) that can be separated by many lines shown in brown and graph b shows the classes separated by the support vectors. In graph a, the lines shown in green are the hyperplanes that are used to separate the classes. Although all the hyperplanes in graph a can separate the classes, the optimal hyperplane in graph b separates the classes with better accuracy. The optimal hyperplane is identified with the aid of the support vector. The support vector determines the maximum margin of each class, which is used to determine the optimal hyperplane. The hyperplane is determined by applying an appropriate kernel type.

The kernel type can be used to solve both linear and non-linear related problems. By incorporating diverse kernel types, both linear and non-linear related problems can be solved. The non-linear associated kernel problems are unravelled by projecting the training data into a high-dimensional feature space (Bruzzone & Persello, 2009), as shown in Figure 2-14.

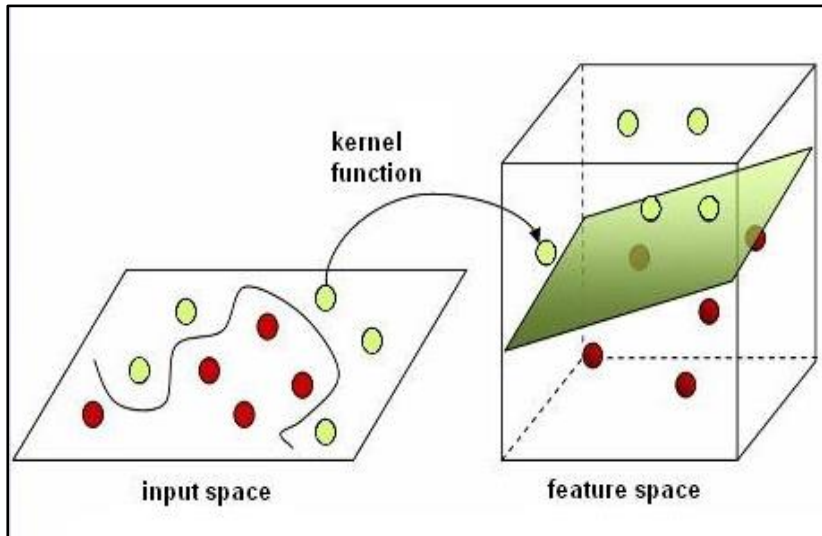


Figure 2-14: Projecting the training data into a high-dimensional feature space (source: <http://i.imgur.com/WuxyO.png>).

Figure 2-14 above shows an example of projecting training data onto a high dimensional space to improve the class separability. This makes the SVM classifier a commonly used algorithm.

Although many kernel types exist, eCognition utilises only the linear and radial bias function kernel (RBF). RBF requires the user to define two (2) inputs, namely cost of constraint (C) and gamma (g), while linear kernel requires one input, namely cost (C). The C parameter controls the classification errors associated with the training data, g determines the extent of the influence of support vectors on the boundary (Edregosa et al., 2011). Hence, high g values imply the support vector and boundary of decision are close. Also, low C values suggest a poorly fitted model, while high C values indicate an overfitted model (Bruzzone & Persello, 2009).

To determine the optimal C and g parameters to be used for the classification, a parameter tuning experimentation was developed in python using the training and validation data created in section 2.6.4. The training/validation data was loaded into a python environment. The scikit-learn package, one of the packages used for machine learning tasks in python, was used. The SVM classifier was called from the Scikit-learn package. The input dataset had different ranges; while the red, green, and blue bands are between 0 and 255, the GLDV contrast is between 1 and 8240. Hence the dataset was normalized to have the same range (0 – 1) to optimise the model training (Hsu et al., 2003). After normalizing the data, the parameter tuning workflow was designed to consider linear and radial basis function (RBF) kernel types, different regularisation (C), and gamma.

Two kernel types were used in the experimental setup to determine the best kernel type for the input dataset. For the C , I tested the following values: 1, 10, 20, 50, 100, 200, 500, 1000; and tested 0.001, 0.01, 0.1, 0.2, 0.3, 0.4, 0.4, 0.5, 0.5, 0.6, 0.7, 0.8, 0.9 for g .

The parameter tuning aims to identify the best combination of features and parameters to obtain the best classification output. Although different feature combinations can identify a specific species, the study was

carried out to determine the best classification accuracy while identifying the individual species that can be mapped with high accuracy. The best overall classification output implies most tree species were correctly classified. The features were added while observing the overall accuracy produced from the resulting parameters to identify the highest classification accuracy resulting from the features used. The best features were then recorded to be used for classification in eCognition.

Appendix 3 shows the features per seasonal dataset used for the tree species classification while the parameter for the classification is shown in Table 2-6 below.

Table 2-6: Parameters per seasonal dataset for SVM classification

Season	Kernel type	C	Gamma
Winter RGB	Radial basis function	0.6	100
Spring RGB	Radial basis function	0.3	10
Summer RGB	Radial basis function	0.1	10
Fall RGB	Radial basis function	0.1	10
Summer MSS	Radial basis function	0.2	10
Combination of RGB Summer and MSS Summer	Radial basis function	0.1	10

The parameters per seasonal dataset shown in Table 2-6 above were recorded to be used for the classification task.

A variable was created in eCognition to save all the configurations during the training process. With the best parameters per season determined, the supervised classification algorithm was loaded, and the training operation was chosen to train the model. The created variable is loaded in the configuration tab. The features that resulted in the best classification accuracy during the parameter tuning were selected as the feature to use. The features were then normalised, and the SVM classifier was chosen. The kernel type, gamma, and C, which were obtained during the parameter tuning to get the best classification accuracy were then entered.

Based on the configuration, the model was trained, and the configuration was saved. The supervised classification algorithm was loaded, and the apply operation was selected. The variable that now has the training configuration was loaded and executed to obtain the classified tree species. The algorithm to apply the model is shown in the Appendix.

The tree species classification was carried out for the winter, spring, summer, and fall RGB datasets. The summer MSS dataset and a combination of summer MSS and Summer RGB were also classified.

2.6.8. Classification accuracy assessment

The classification accuracy was estimated by comparing the classified tree species to the validation samples to generate an error matrix. The user accuracy (UA), producer accuracy (PA), overall accuracy (OA), kappa statistics (k), and F measure were estimated.

The OA was estimated by the ratio of the sum of the major diagonal to the total number of samples. The UA was estimated by the ratio of the number of correctly classified samples for every class to the total number of samples that have been classified as that class, while the PA was estimated by the ratio of the

number of rightly classified samples for every class to the total number of samples for that class. The kappa statistics and F measure was estimated using equation 4 and 5 below.

$$k = \frac{(\textit{observed accuracy} - \textit{chance agreement})}{(1 - \textit{chance agreement})} \quad \text{eqn 5}$$

$$F \textit{ measure} = 2 * \frac{(UA * PA)}{(User \textit{ accuracy} + Producer \textit{ accuracy})} \quad \text{eqn 6}$$

Each accuracy assessment provides different information. The overall accuracy gives a general overview of the classification result but does not give any class information about error or accuracy. However, the user accuracy and producer accuracy provide such information. The user accuracy indicates how representative the classified map is on the ground, while producer accuracy refers to the accuracy based on the classification. The overall accuracy indicates the general classification error. On the other hand, Kappa statistics indicate the classification that was in agreement with the validation data and the agreement by chance (Congalton & Green, 2019). F measure also provides a means to combine PA and UA into a single measure that depicts both accuracies.

3. RESULTS

This chapter presents the results based on the objectives (i.e., image segmentation, classification, and accuracy assessment).

3.1. Segmentation of images

3.1.1. Multi-resolution segmentation

The scale parameters mentioned were used in the multi-resolution segmentation for all input images through a trial-and-error approach to determine the best scale parameter per seasonal dataset. A sample set of the segment created per scale parameter was compared to the tree crowns manually digitised to determine the segmentation accuracy. The best scale parameter produced the lowest segmentation error compared to the other parameters when the segmentation accuracy was estimated. The parameters used for the segmentation is shown in Table 3-1 below.

Table 3-1: Segmentation parameters used for all seasonal datasets

	Summer RGB	Winter RGB	Spring RGB	Fall RGB	Summer MSS	Summer RGB and MSS
scale	72	40	58	65	74	70
Shape	0.6	0.6	0.6	0.6	0.6	0.6
compactness	0.8	0.8	0.8	0.8	0.8	0.8

After obtaining the multi-resolution segmentation algorithm parameters, the algorithm was executed to get the image segments. Figure 3-1 below shows a sample segmentation for the RGB fall dataset.

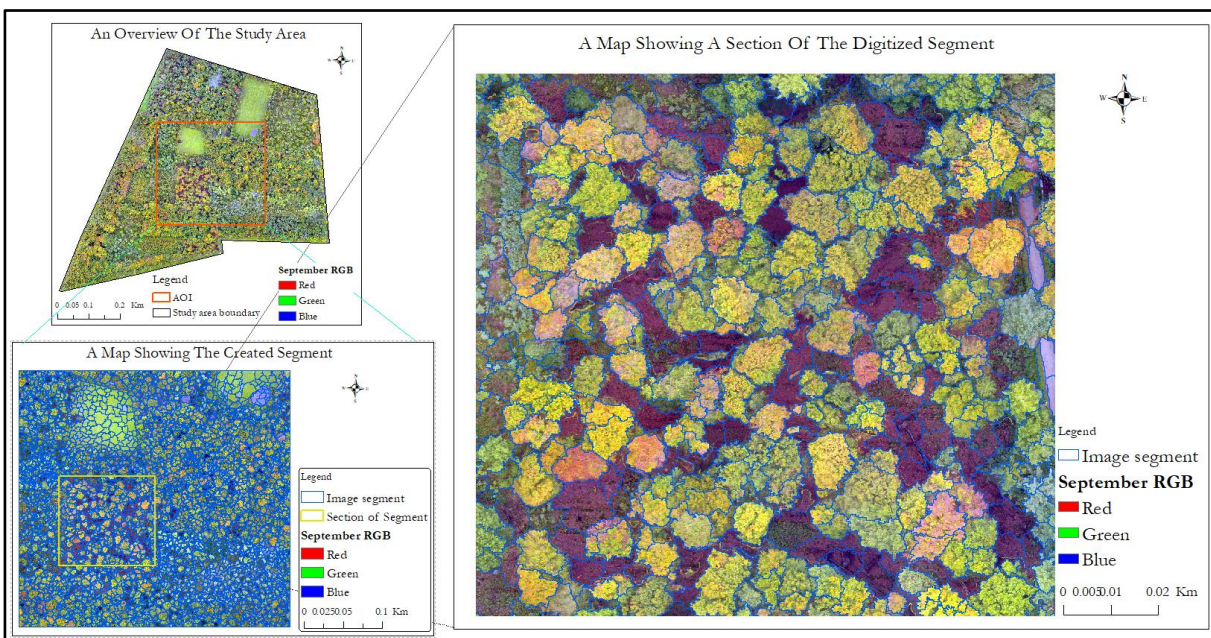


Figure 3-1: Segmentation output for UAV-RGB fall dataset.

From Figure 3-1 above, some under-segmentation and over-segmentation can be observed. This research was conscious of the fact that there are no flawless parameters when segmenting image objects. Creating image segments when using even the optimal parameters will always result in some under-segmentation and over-segmentation. However, it is essential to reduce the segmentation error to the minimum possible.

The other segmentation results are shown in the Appendix.

3.1.2. Accuracy assessment of segments

The segments produced from the multi-resolution segmentation were compared to the digitised segments using equation 3 (refer to section 2.7.1).

Due to under segmentation and over-segmentation observed in Figure 3-1, there is the need to estimate the overall accuracy of the image segment. The under segmentation (equation 2) and over-segmentation (equation 1) was calculated and used as input to determine segmentation error (equation 4). Table 3-2 below shows the segmentation error and accuracy per dataset.

Table 3-2: Segmentation accuracy of all input datasets

	Winter RGB	Spring RGB	Summer RGB	Fall RGB	Summer MSS	Summer MSS and RGB
Total segmentation error	0.69	0.43	0.24	0.27	0.18	0.29
Segmentation accuracy	0.31	0.57	0.76	0.73	0.82	0.71

Table 3-2 above shows that the summer UAV-MSS dataset resulted in the lowest segmentation error of 0.18, while the summer UAV-RGB dataset had the lowest segmentation error of 0.24 among the RGB datasets. The Winter dataset had the highest segmentation error of 0.69, while the spring UAV-RGB dataset resulted in 0.43. The combination of summer MSS and RGB produced a segmentation error of 0.29.

3.2. Tree species classification

Features per seasonal dataset shown in Appendix 3 and parameters from Table 2-16 were used for the seasonal tree species classification.

3.2.1. Summer UAV-RGB tree species classification

The result of the summer UAV-RGB tree species classification is shown in Figure 3-3 below.

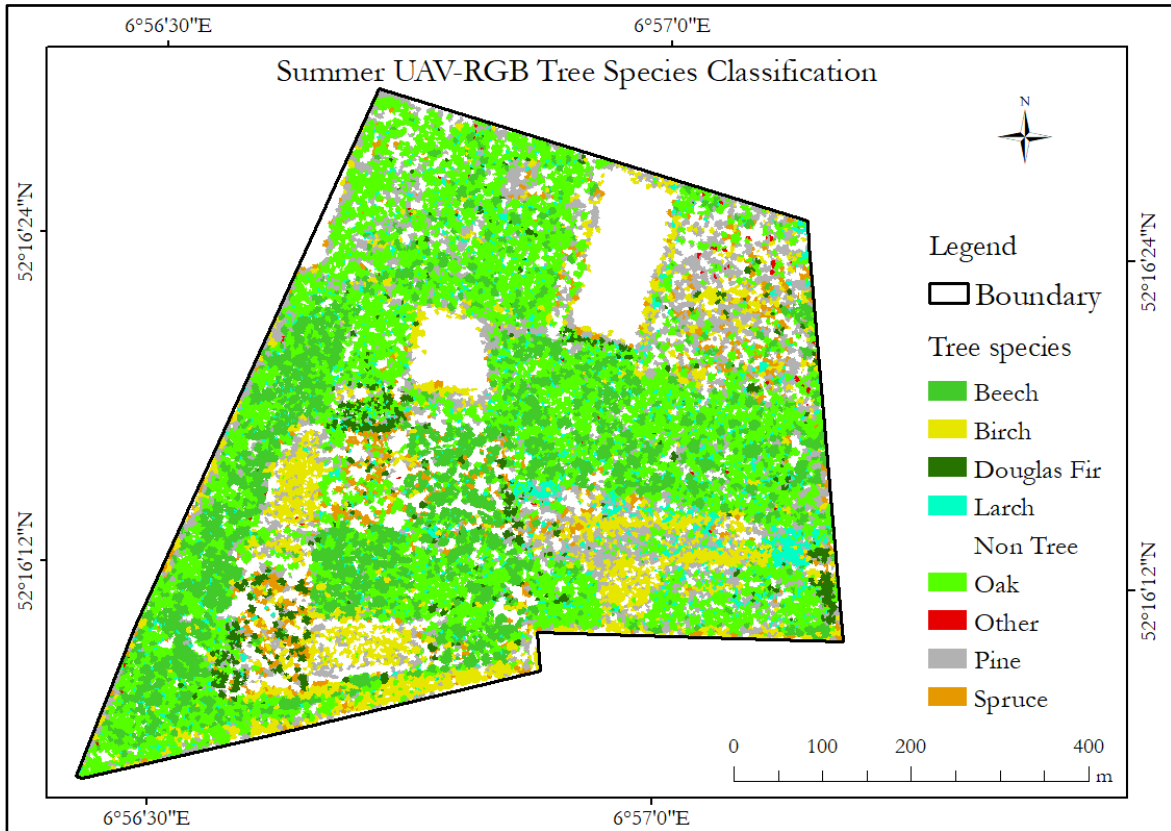


Figure 3-2: Summer UAV-RGB tree species classification

Figure 3-3 above is the summer tree species classification, which shows a good tree species distribution. Oak was the major tree species in the study area, as can be seen in Figure 3-3 above. Misclassification can be observed between beech and most of the tree species, with the main misclassification between oak and beech. The non-trees were mostly misclassified.

During the field work, larch was identified in the middle and lower right section of the study are and this was also classified. Douglas Fir can also be identified in the middle section of the study area. Pine is distributed in the lower section of the study area. Birch seems to be over-classified, while most of the other tree species were misclassified.

Comparing the UAV RGB dataset, the summer tree species classification produced the best classification.

3.2.2. Winter UAV-RGB tree species classification

The result of the winter UAV-RGB tree species classification is shown in Figure 3-4 below.

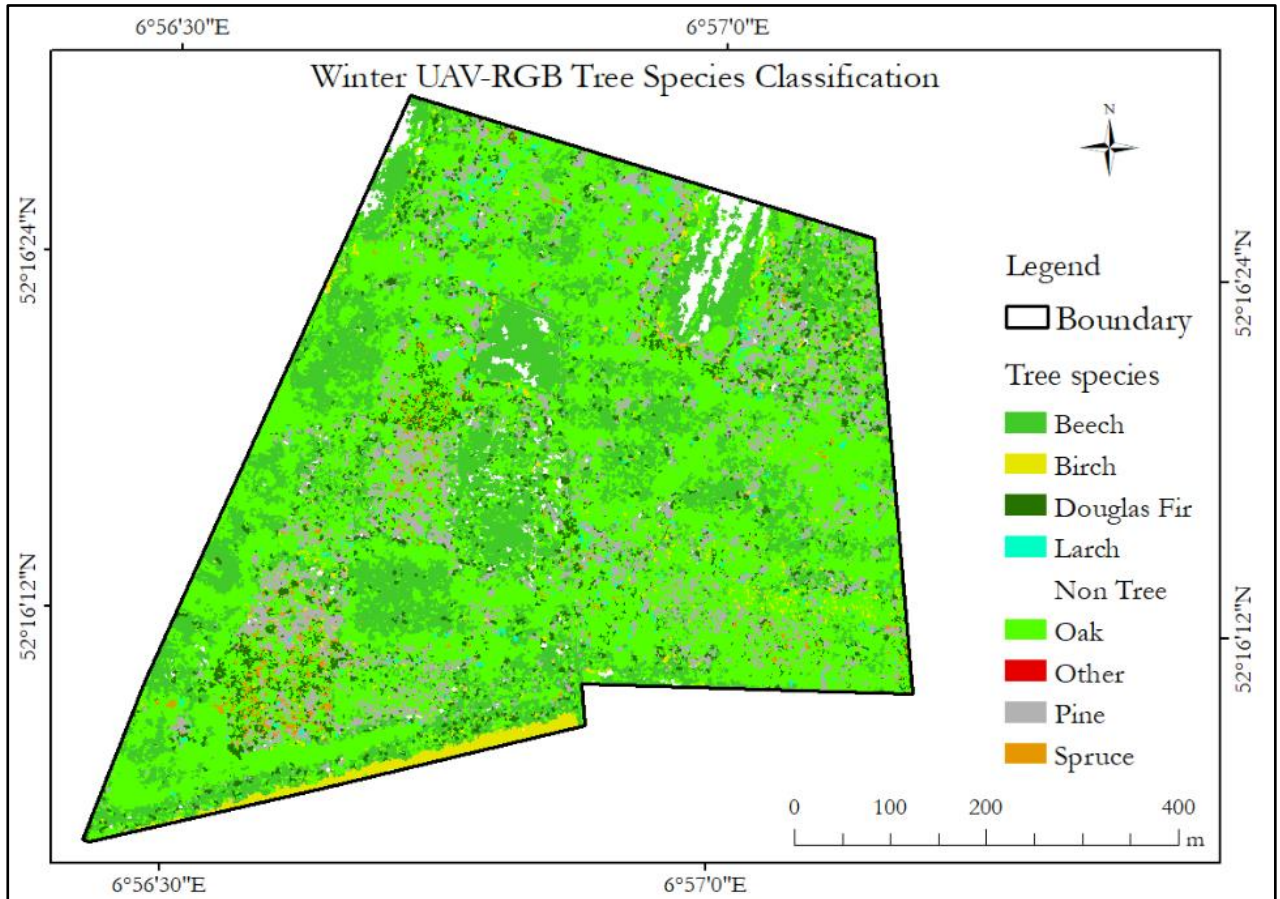


Figure 3-3: Winter UAV-RGB tree species classification

Figure 3-4 above is the winter tree species classification, which shows a poor tree species classification. Misclassification can be observed between oak and most tree and non-tree species. Some of the non-tree identified in the summer was classified predominantly as oak and beech, which was an error. Most of the larch at the central part of the area was also not identified in the winter. Figure 3-4 above shows undesirable results for the tree species classification. Comparing with the other seasonal dataset, the winter UAV-RGB dataset produced the worst tree species classification.

Although the tree species was mostly misclassified, the birch at the lower-left corner was identified.

3.2.3. Spring UAV-RGB tree species classification

The result of the spring UAV-RGB tree species classification is shown in Figure 3-5 below.

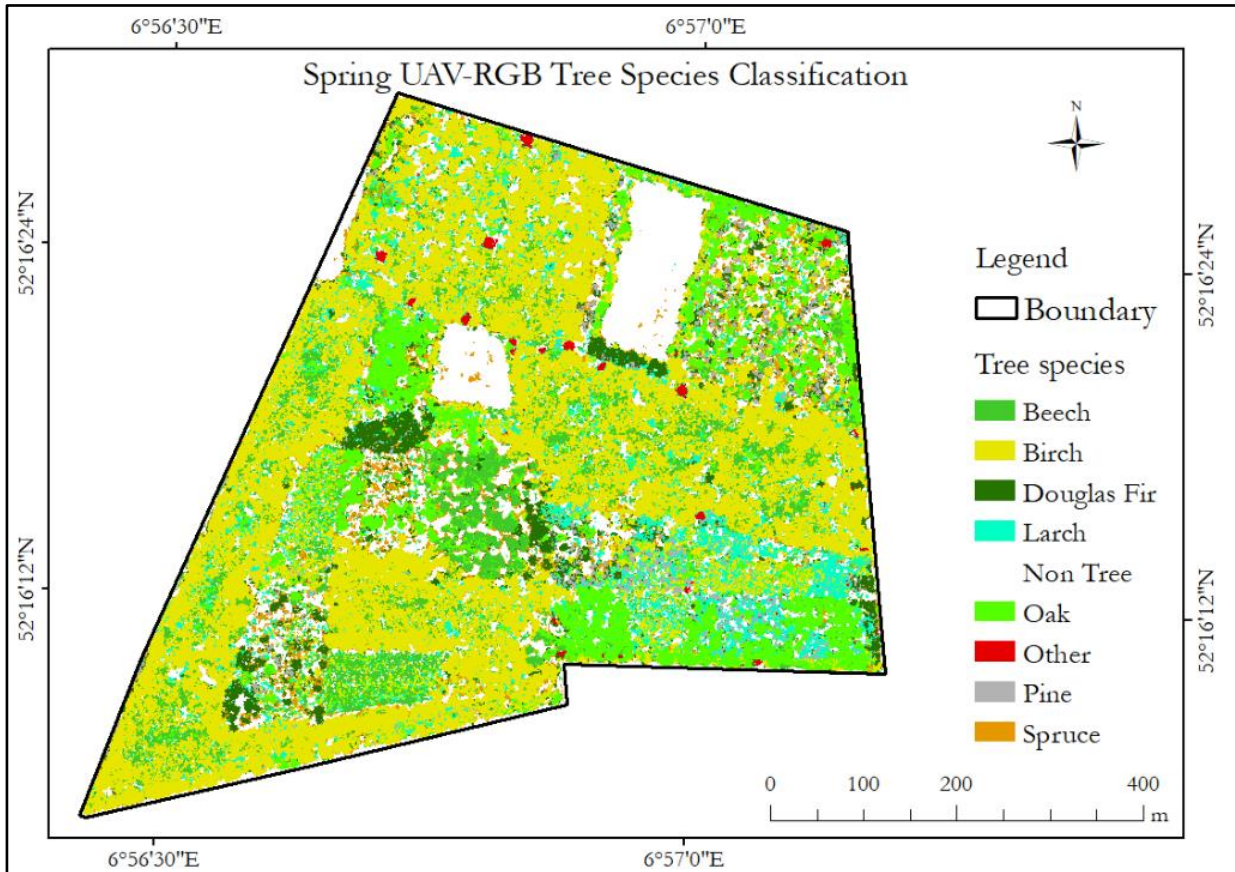


Figure 3-4: Winter UAV-RGB tree species classification

From Figure 3-5 above, spring tree species classification shows misclassification of the birch tree species. From the field visit and summer RGB classification, oak was the dominant species and not birch as depicted by the spring dataset. Other tree species were identified in the spring dataset better than in the summer and winter datasets. Oak was under-classified. Non-tree was predicted with a higher degree in the spring dataset than in the summer dataset. Pine, Douglas fir, and spruce were also misclassified; however, larch in the lower left side was identified.

3.2.4. Fall UAV-RGB tree species classification

Figure 3-6 below is the result of the spring tree species classification.

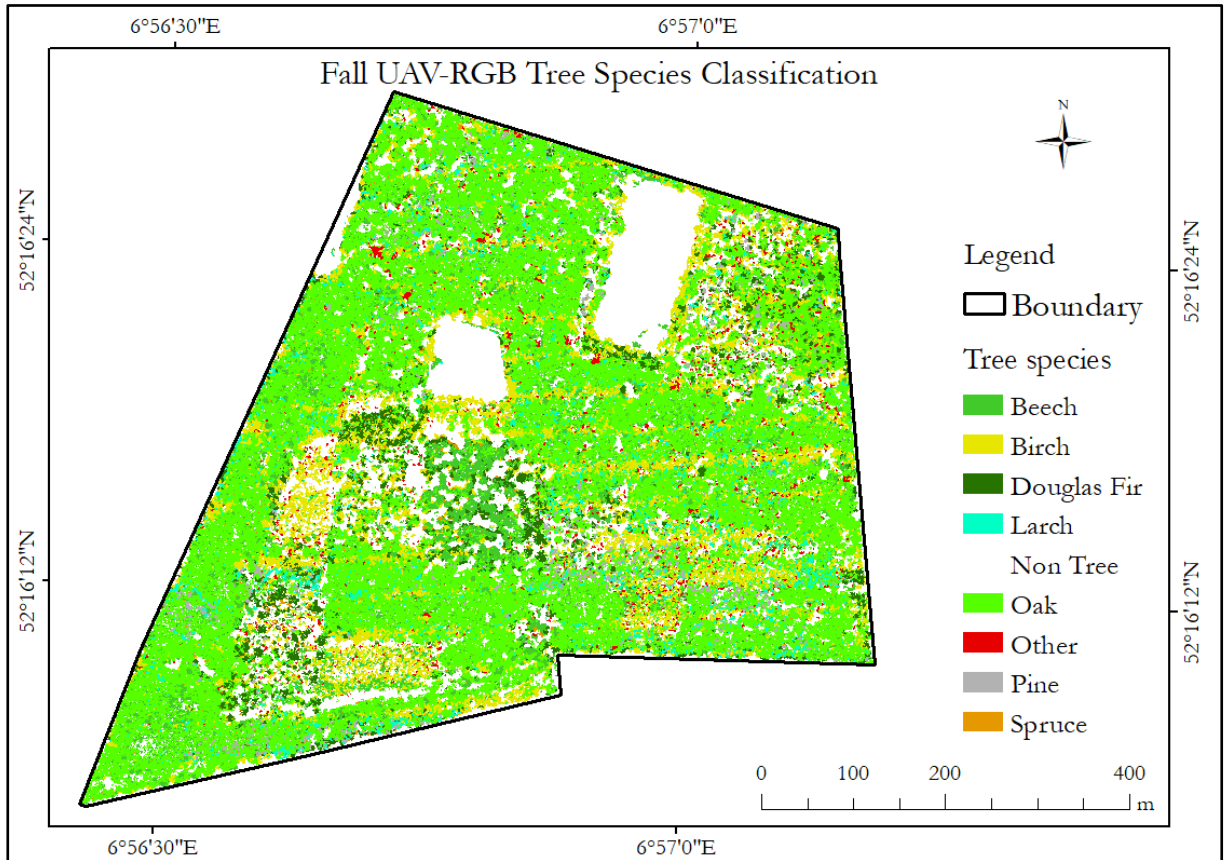


Figure 3-5: Fall UAV-RGB tree species classification

From the fall tree species classifying shown in Figure 3-6 above, oak can be seen taking over most classes in the fall classification result. The misclassification is seen more between oak and beech. The non-tree class was predicted better when compared to the winter dataset. The prediction of birch was improved in the fall dataset when compared to the spring dataset. The larch in the lower left was misclassified.

3.2.5. Summer UAV-MSS and combination of RGB and MSS tree species classification

The result of the tree species classification is shown in Figure 3-7 below.

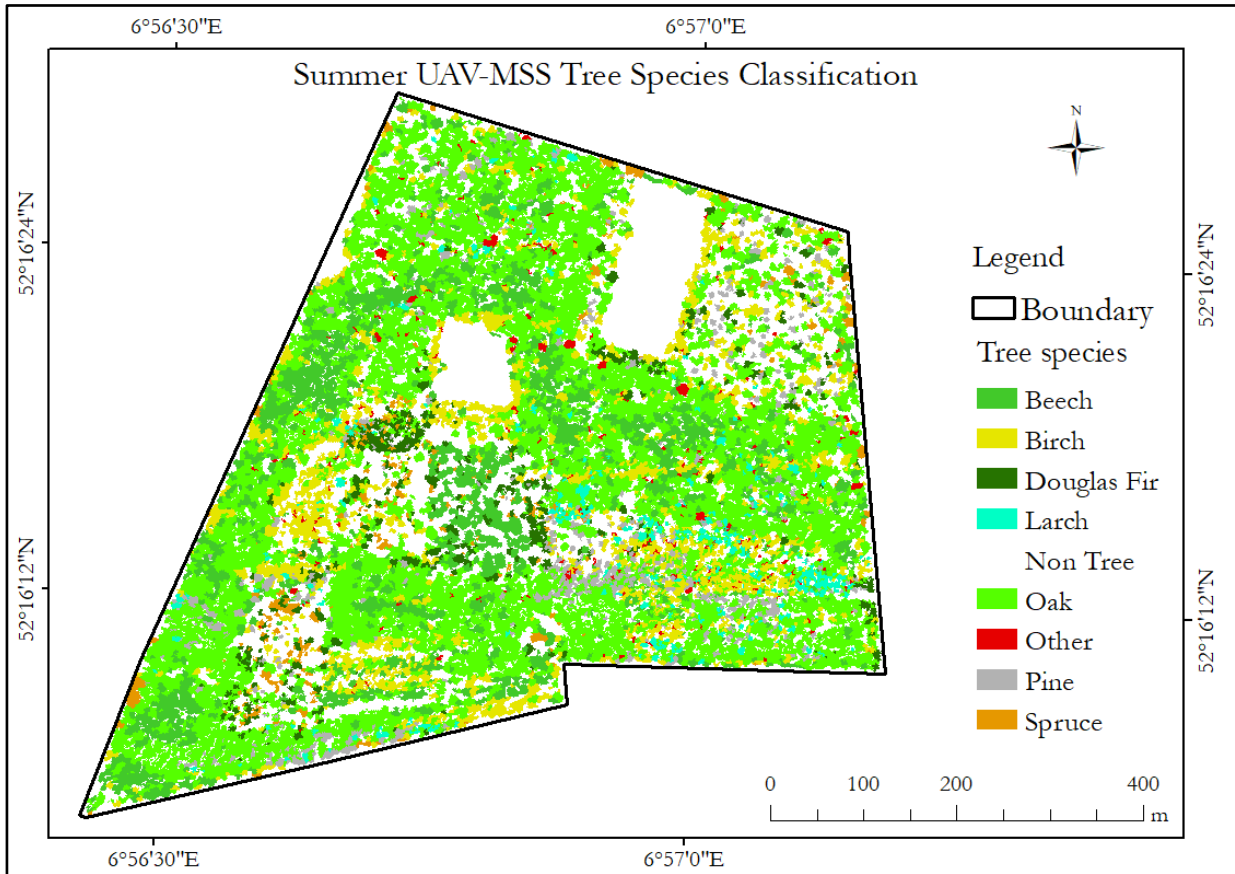


Figure 3-6: Summer UAV-MSS tree species classification

The summer UAV MSS classification shows a better classification of the tree species when compared to the other UAV-RGB datasets. Non-tree was correctly predicted. The distribution and location of larch and birch agree to what was observed on the field. The spruce at the lower-left corner was predicted accurately by the MSS dataset but not by any of the UAV-RGB datasets.

The summer UAV-RGB and MSS result does not vary much except for some little change in the distribution of the tree species. The result of the tree species based on the combination of UAV-RGB and MSS is also shown in Figure 3-8 below.

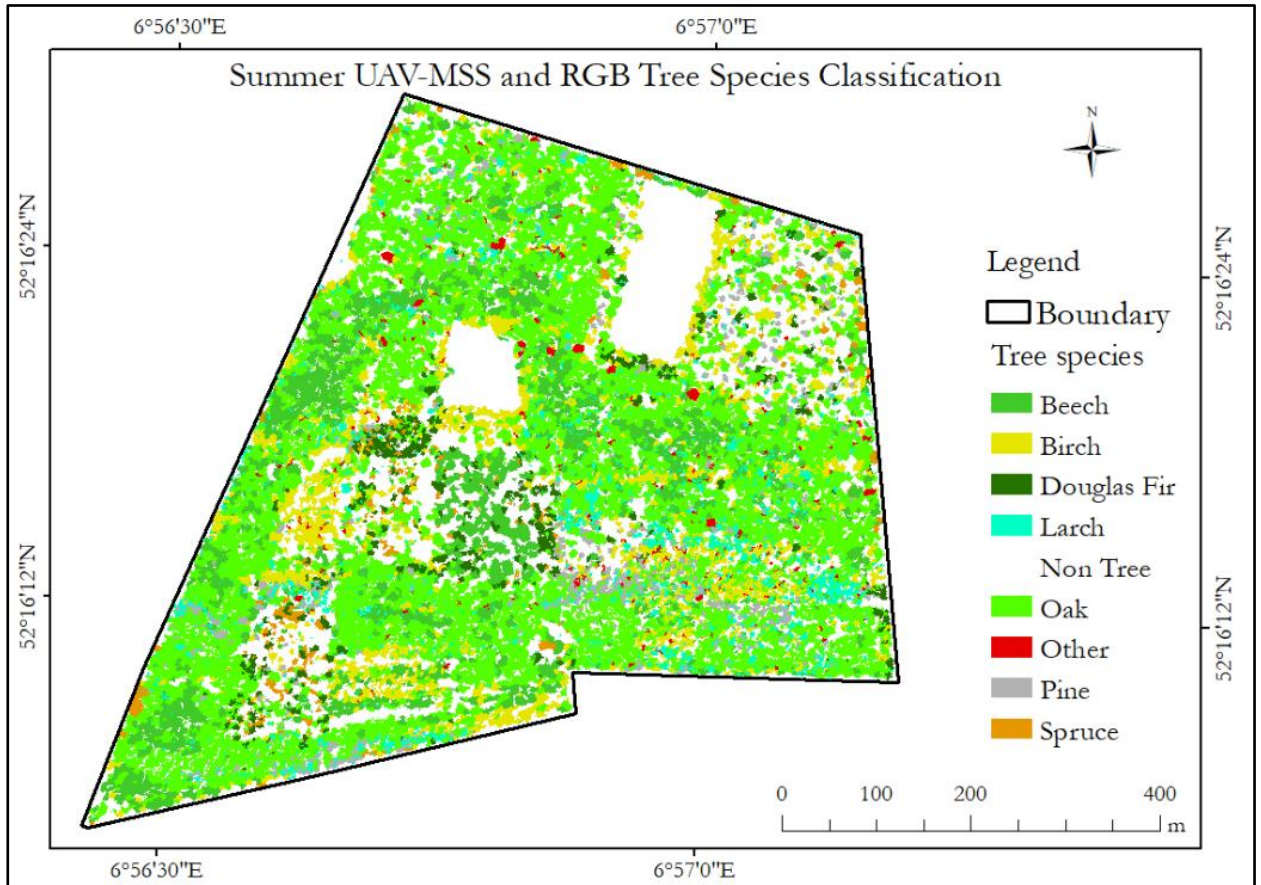


Figure 3-7: Tree species classification of fall UAV -RGB dataset.

3.3. Accuracy assessment

The user accuracy, overall accuracy, overall accuracy, and kappa statistics are shown in Table 3-3 below.

Table 3-3: Tree species classification accuracies for all datasets.

Category	Class	Accuracy											
		User accuracy						Producer accuracy					
		Winter	Spring	Summer	Fall	MSS	MSS + RGB	Winter	Spring	Summer	Fall	MSS	MSS + RGB
Broadleaf	Beech	0.42	0.9	0.84	0.85	0.94	1	0.38	0.93	0.62	0.71	0.74	0.74
	Oak	0.32	0.68	0.61	0.56	0.72	0.74	0.72	0.89	0.85	0.82	0.91	0.98
	Birch	0.72	0.56	0.68	0.74	0.69	0.87	0.3	0.81	0.7	0.79	0.9	0.9
Coniferous	Larch	0.62	0.78	0.91	0.64	0.81	0.85	0.3	0.83	0.77	0.56	0.81	0.85
	Douglas Fir	0.48	0.67	0.78	0.82	1	0.92	0.39	0.9	0.84	0.62	0.86	0.89
	Pine	0.46	0.54	0.81	0.55	0.93	0.9	0.34	0.69	0.81	0.66	0.84	0.88
	Spruce	0.58	0.62	0.9	0.6	1	0.96	0.16	0.7	0.69	0.36	0.85	0.88
	Other	0	0.83	1	1	1	1	0	0.42	0.4	0.25	0.4	0.6
	Non tree	0.5	0.83	0.93	0.78	0.97	1	0.3	0.93	1	0.89	1	1
		Overall accuracy						KIA					
		0.39	0.64	0.77	0.68	0.84	0.88	0.28	0.59	0.74	0.63	0.81	0.86

From Table 3-3 above, the overall accuracy (OA) of RGB, spring RGB, summer RGB, fall RGB, summer MSS and combination of summer MSS and RGB were 0.49, 0.64, 0.77, 0.68, 0.84, and 0.88 respectively. The highest classification accuracy for the RGB dataset was Summer (0.77), with winter showing the lowest classification accuracy (0.49). Both MSS datasets (MSS alone and RGB and RGB) show higher accuracy than the RGB dataset. However, the combination has higher accuracy than the MSS classification alone.

The MSS and RGB dataset combination accurately identified beech and others, while the MSS accurately identified spruce and others.

Oak showed the most misclassification when observing the spring, summer, and summer RGB and MSS combination. The highest misclassification for the summer RGB was identified to be between beech and oak, with about 15% of oak samples classified as beech and 61% of oak correctly classified. The spring RGB accuracy also shows high misclassification between beech and oak, about 15% of the oak was classified as beech, and 68% of the oak was correctly classified. The remaining oak misclassification was observed between non-tree, other, pine, birch, and larch. About 14% of the oak tree species data was classified as beech, and 74% of the oak was correctly classified according to the combination of summer RGB and MSS accuracy.

The winter RGB resulted in the least classification accuracy, hence the most misclassification. Oak, other, non-tree, pine, birch, and spruce tree species were observed as the tree species with the highest misclassification in the fall RGB, as can be seen from accuracy table. About 46% and 31% of oak and spruce, respectively, were correctly classified. Also, about 15% of the oak was classified as beech, and 47% of beech was classified as oak. The F measure estimated based on the UA and PA is also shown in Table 3-4 below.

Table 3-4: F measure per tree species per seasonal dataset

		F measure					
Category	Class	Winter	Spring	Summer	Fall	MSS	MSS + RGB
Broadleaf	Beech	0.40	0.91	0.71	0.77	0.83	0.85
	Oak	0.44	0.77	0.71	0.67	0.80	0.84
	Birch	0.42	0.66	0.69	0.76	0.78	0.88
Coniferous	Larch	0.40	0.80	0.83	0.60	0.81	0.85
	Douglas Fir	0.43	0.77	0.81	0.71	0.92	0.90
	Pine	0.39	0.61	0.81	0.60	0.88	0.89
	Spruce	0.25	0.66	0.78	0.45	0.92	0.92
	Other	0.00	0.56	0.57	0.40	0.57	0.75
	Non tree	0.38	0.88	0.96	0.83	0.98	1.00

As shown in Table 3-4 above, the F measure for all tree species in winter was less than 0.5, with oak the best classified and other tree species with the lowest F measure. Comparing all the datasets, birch was best classified in the spring dataset. According to Table 3-3, the MSS outperformed the RGB dataset while the combination of UAV-RGB and MSS also outperformed the MSS. The summer RGB dataset also obtained the highest F measure for 5 of the eight tree species.

4. DISCUSSION

The chapter discusses the results of the study. The primary objective of this research is to assess the performance of multi-seasonal UAV-RGB and UAV-multispectral (MSS) images and their combination for tree species discrimination in a mixed temperate forest using a support vector machine classification algorithm. The first section (4.1) of this chapter reflects on the finding of the first objective. The second section (4.2) reflects on objectives 2, 3, and 4. The limitation of the research is discussed in section 4.3.

4.1. Segmentation accuracy of the seasonal dataset

The first research question was to determine the segmentation accuracy of the seasonal UAV datasets. The results are discussed in 4.1.1 and 4.1.2.

4.1.1. Segmentation of images and accuracy assessment

The MRS accuracy obtained was different per the seasonal dataset. The variation in segmentation accuracy may be influenced by the image resolution, scale parameter, shape, compactness, and segmentation algorithm used (Möller et al., 2007). The difference in tree crown size, little or no gaps between adjacent crowns, lack of ample spectral separation between tree crowns of different species, and variation of spectral separation between tree crowns of the same species also influences the segmentation accuracy (Gomes & Maillard, 2016; Pu & Landry, 2012). The different segmentation accuracy revealed that the tree crown obtained from the image segmentation varies per seasonal dataset.

To determine the influence of seasonality on the input dataset for the segmentation process, the same tree over different seasons was analysed to observe the spectral variation due to phenological changes, as shown in Figure 4-1 below.

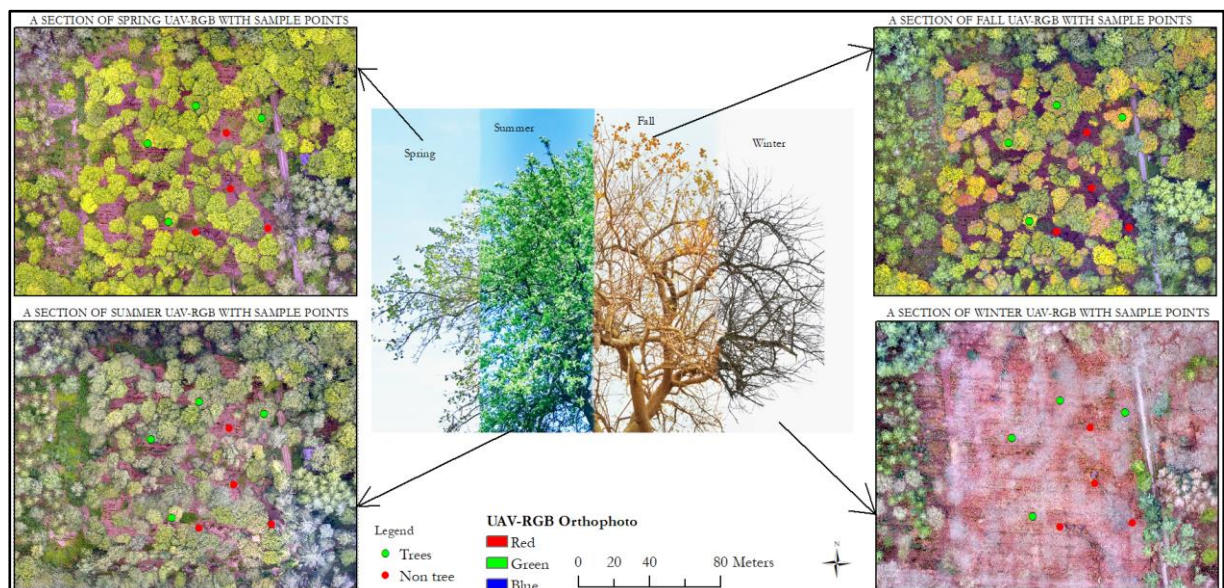


Figure 4-1: Pictorial view of some deciduous tree samples in the four seasons.

Figure 4-1 above shows the different behaviour of deciduous trees in each season. In February, the trees, especially deciduous trees, show different reflectance per season since leaves have fallen off. According to National Geography, each season has its light, temperature, and weather pattern (National Geography,

2021). Winter in the Netherlands is approximately between 21st December to 20th March and is the season where the leaves on deciduous trees are gone. The absence of leaves on deciduous trees results in the UAV sensor imaging the forest floor instead of the leaves, as seen in Figure 4-1 above because the branches on the deciduous trees are empty. This makes it difficult to segment the tree crowns accurately.

Fall is between 21st September and 20th December, and it is the transition from summer to winter. During fall, photosynthetic activities in plants are reduced because daylight becomes shorter, and the temperature becomes considerably colder, unlike in summer (National Geography, 2021). This changes leaf colour and shedding of deciduous tree leaves, thus affecting the segmentation accuracy because the leaf on a particular tree shows different colours, hence different spectral information. Not all leaves on one tree change colour the same day or even week, so the leaf on one particular tree may show different colours, hence different spectral information. The varying spectral details of the same tree may result in splitting the tree crown into different crowns.

Spring is approximately between 21st March to 20th June, and it is the season where trees that shed their leaves start growing their new leaves. In spring, day and night are approximately equally spaced, enabling the plants to get enough light and other conditions favourable for photosynthesis (National Geography, 2021). Fresh leaves come out but not all at the same time, some species start earlier than others. In one crown, all the leaves on the branches have the same colour but the colour may not all come at once. Those at the end of branches usually come a bit later. The different colours of leaves in each season at different phenological stages affect the tree's spectral signature. Figure 4-2 below shows an example of under segmentation and over-segmentation.

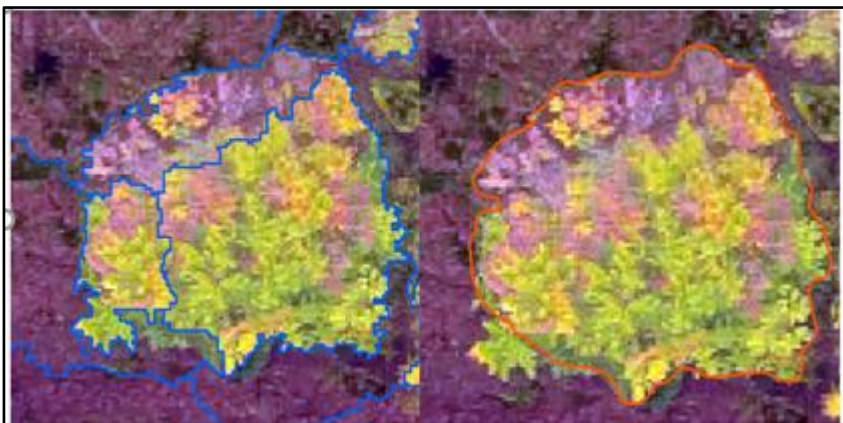


Figure 4-2: Comparing MRS segments (blue) and manually digitized segment (red) for under segmentation and over-segmentation of tree crown.

Figure 4-2 above shows under segmentation and over-segmentation caused by the phenological changes of the tree species. The spring and fall RGB dataset mostly underestimate tree crown created.

Summer yields higher segmentation accuracy for the RGB dataset. This can be attributed to the fact that the leaves in one tree have mostly regained uniform colour, and different species may have slightly different colours. While some tree species are reddish, others are bright green, yellow-green, and dark green, which the UAV sensor can detect. Hence, this improves the segmentation process for the summer dataset.

The UAV-MSS dataset resulted in a higher segmentation accuracy than the UAV-RGB dataset, although both datasets were obtained in Summer. The MSS dataset has bands such as red edge and near infra-red, which aids the tree crown segmentation by improving the difference between the tree species. Also, the

MSS dataset is a 16-bit integer dataset, making it possible to store an extensive range of values compared to RGB, which is 8 bits. The bands and storage capacity of the MSS dataset make it possible to represent different trees with values unique for each object, hence improving segmentation accuracy.

Although UAV-MSS data type makes it possible to identify different features, combining it with UAV-RGB results in image objects with a higher segmentation error (0.29) than the UAV-MSS segmentation error. The high error for the summer MSS and RGB combination may be due to the different values for the same feature. While the blue band from the RGB dataset is an 8-bit integer data (storing values between 0 and 255), the MSS dataset is a 16-bit integer data (storing values between 0 and 65535). The different values per band per tree crown may influence the segmentation process as the same tree crown may show different value ranges.

To observe the difference in the digital number (DN) between the MSS and RGB datasets, the DN numbers are observed between red and green bands of the RGB and MSS dataset, as shown in Figures 4-3 below.

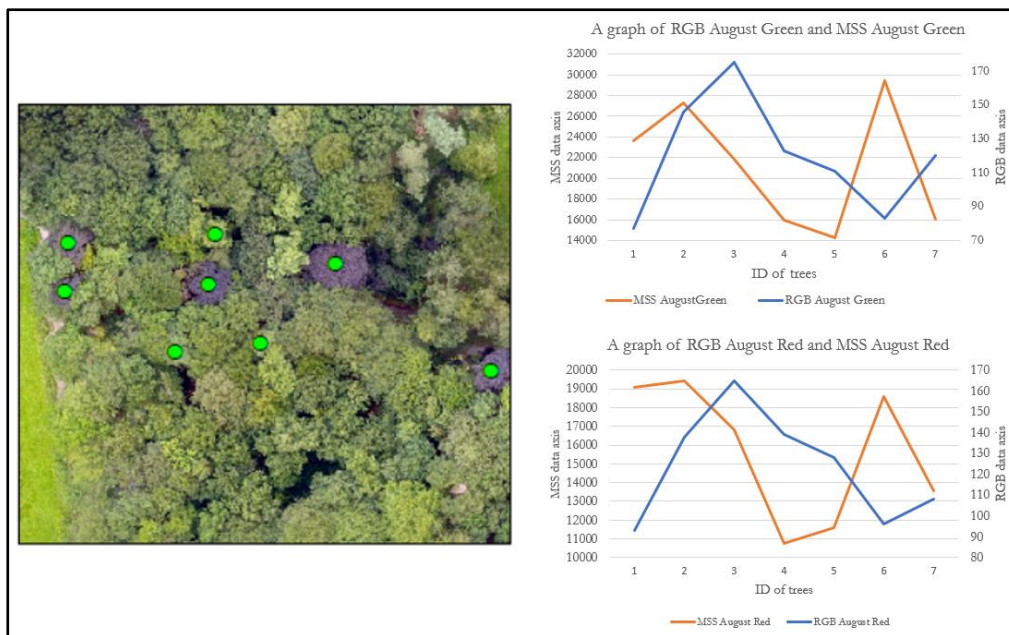


Figure 4-3: Comparison of Summer RGB and MSS Red and Green dataset for some selected trees

From Figure 4-3 above, Tree 1 has 77 and 93 for Summer RGB Green and Red respectively, while Summer MSS Green and Red values were 23,664 and 19,066. These are DN for the same trees, but the difference in data type results in different values for the same trees, which may confuse the segments created.

All the seasonal datasets were resampled and filtered before the image segmentation to reduce the noise inherent in very high-resolution imagery. Resampling the imagery to 10 cm is inconsistent with research carried out by Okojie (2017), who reported that 30 cm is suitable for tree crown segmentation. However, this research was carried out in a forest comprising both old and young forests. However, this is consistent with research carried out by Gaden (2020) on the same study area. Filtering the images reduces under segmentation, improving the overall segmentation as the filtering averages the spectral values (ZhiYong et al., 2018). This is consistent with Esong Effiom (2018) research, which reported that resampling and filtering very high resolution satellite images prior to segmentation improve segmentation accuracy.

4.2. Tree species classification of UAV-RGB dataset

The second research question was to determine which season UAV-RGB yield the highest segmentation accuracy in separating the tree species. The results are discussed in 4.2.1 below.

4.2.1. UAV-RGB tree species classification

The summer UAV-RGB dataset resulted in the highest overall classification accuracy (0.77) among the UAV-RGB dataset. From the F measure, the summer dataset had a high F measure for 5 of the 8 tree species, with spring having a high F measure of 2 tree species (oak and beech) and fall with a high F mask for birch.

When looking at the individual species, most of the misclassification was observed between oak and the other tree species, however the dominant confusion between oak and beech. This is consistent with research carried out by Bjerreskov et al. (2021), who also reported high errors between oak and other tree species. The confusion may be related to oak and beech being the two dominant tree species in the study area. Also, the colour of beech and oak in summer are similar, as shown in Figure 4-4 below.

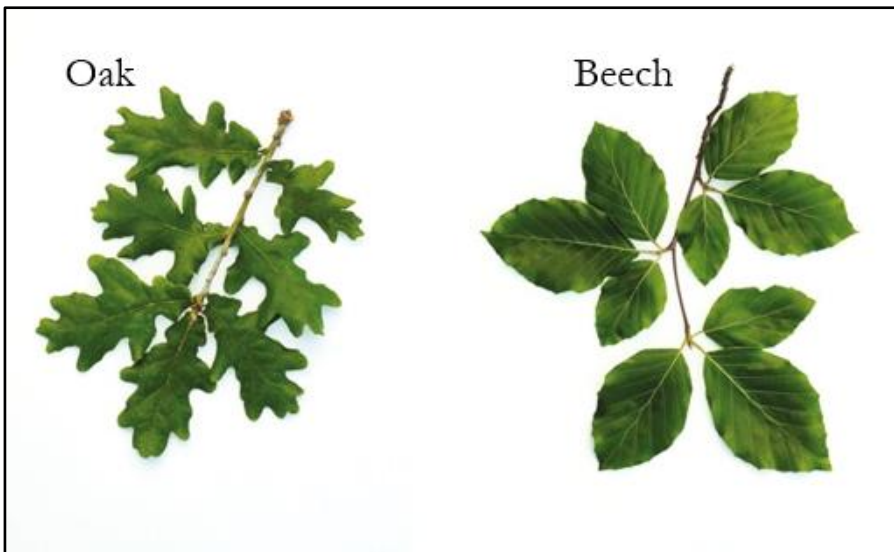


Figure 4-4: Oak and beech profile of all features used for summer UAV-RGB dataset.

From Figure 4-4 above, the colour of oak and beech are very similar; hence both tree species show similar spectral reflectance. It is, therefore, difficult to separate oak and beech using spectral features as shown in Figure 4-5 below.

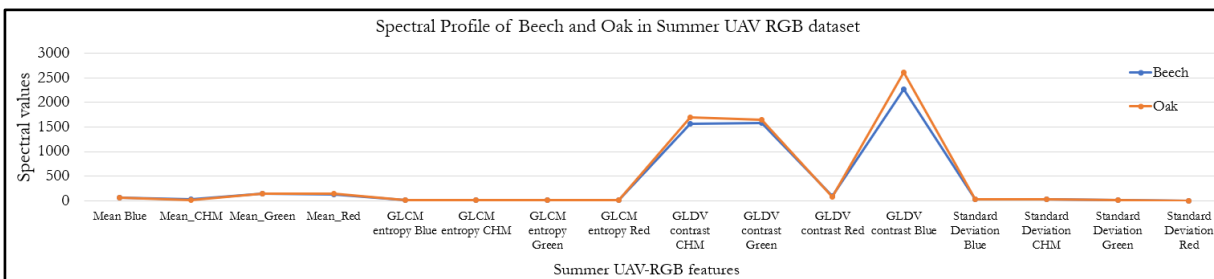


Figure 4-5: Oak and beech profile of all features used for summer UAV-RGB dataset.

From Figure 4-5 above, all the spectral features (mean and standard deviation) used showed little or no separability because both trees species have similar colours hence similar spectral reflectance and features.

GLDV contrast (especially GLDV contrast blue), a texture feature, shows separability between oak and beech. Beech has a fine texture, while oak has a coarse texture (Rocheleau, 2009). The difference in the texture of oak and beech is identified by GLDV contrast. GLDV contrast blue shows the highest separability, followed by GLDV contrast CHM, GLDV green, and GLDV contrast red. Hence, to classify beech and oak only in the study area, a GLDV contrast of blue and CHM could be used.

However, beech and oak are not the only tree species to classify. Hence features that can identify many tree species present and improve the overall classification accuracy was added. Although the spectral features could not differentiate oak and beech, they can separate spruce, birch, Douglas fir, larch and pine as shown in Figure 4-6 below.

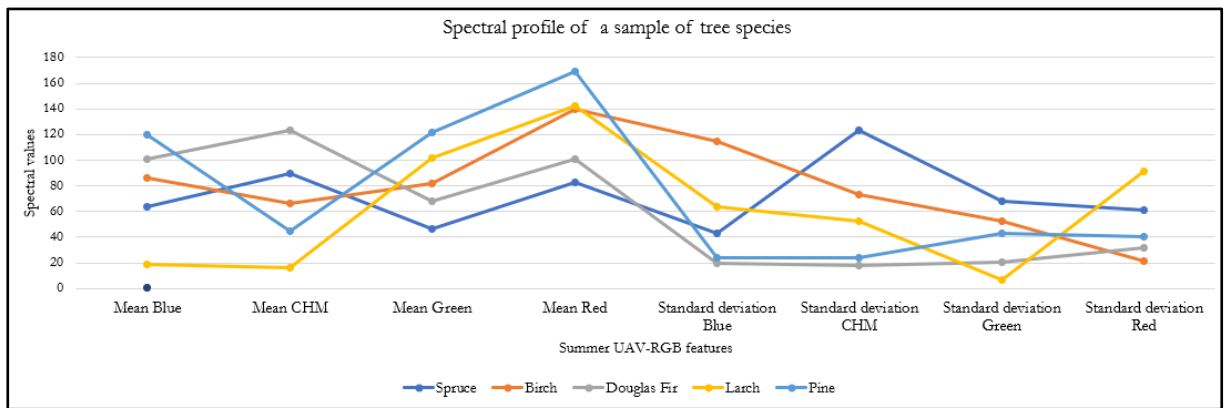


Figure 4-6: Spectral profile of some features and tree species

Figure 4-6 above shows some tree species class separability using the mean and standard deviation of green, blue, CHM, and red. According to Figure 4-6, some level of separability can be observed between larch, birch, pine, Douglas fir, and spruce when the mean blue band and CHM are used. However, low separability exists when the mean and standard deviation of the red, green, CHM, and blue bands were observed in Figure 4-5. To identify the diverse tree species present, a compromise was made such that the features that identified most of the tree species with higher overall accuracy were used.

The summer dataset were inconsistent with research suggesting that the mid and late spring mono-temporal dataset yields the best tree species classification accuracy (Weil et al., 2017; Grybas & Congalton, 2021). The disparity may be attributed to the different tree species under consideration. Also, the different type of forest used for the study may contribute to the disparity as the complexity of the forest contributes to the accuracy of the tree species.

Larch also shows high accuracies (UA, PA, and F measure) for spring and summer seasonal dataset indicating that Larch is best classified in spring and summer. Larch is a deciduous tree which looks like an evergreen tree in the spring and summer. The needles of larch in spring and summer are green but these needles turn to bright yellow in fall and drops in the winter. Larch was expected to yield high accuracy in fall due to distinct bright yellow needles, however, the accuracy of larch in spring and summer was higher than that in fall as shown in Figure 4-7 below.

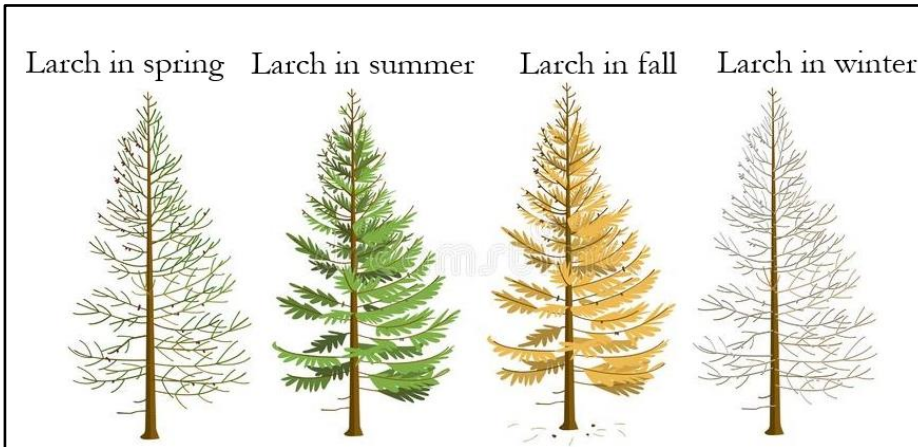


Figure 4-7: Larch in spring, summer, fall and winter.

Although Figure 4-7 shows the distinct yellow needles of larch, this was not identified by the UAV probably due to the time the image was obtained. The fall image was obtained on 12th October, which is about 3 weeks in fall season. The distinct bright yellow needles may not have completely turned. Hence this may affect the accuracy of larch.

The F measure accuracy matrix shown in Table 3-3 shows that the deciduous tree species in general shows higher accuracy than the evergreen tree species in winter. The result is inconsistent with research carried out by Kim et al. (2009), who reported that leaf off (winter) season images improve coniferous tree species classification. Persson et al. (2018) also classified tree species using multi-temporal Sentinel 2 and commented that coniferous tree species were best classified during the leaf offseason.

Although oak and beech are the two main dominant species, birch produced the highest user accuracy among the winter tree species. This can be attributed to the fact that when birch tree shed their leaves in the winter season, the needles on the birch remain and this usually has a distinct white colour. Figures 4-8 below shows sample of birch trees from the UAV images.



Figure 4-8: Birch trees in winter

Figure 4-8 above shows a section of birch trees from the winter UAV orthophoto. The distinct colour of birch in winter makes it possible to identify them compared to the other tree species. GLCM contrast is

the feature that shows the highest separability between birch and the remaining tree species in winter. Figure 4-9 below shows the spectral profile of GLCM contrast for all three species.

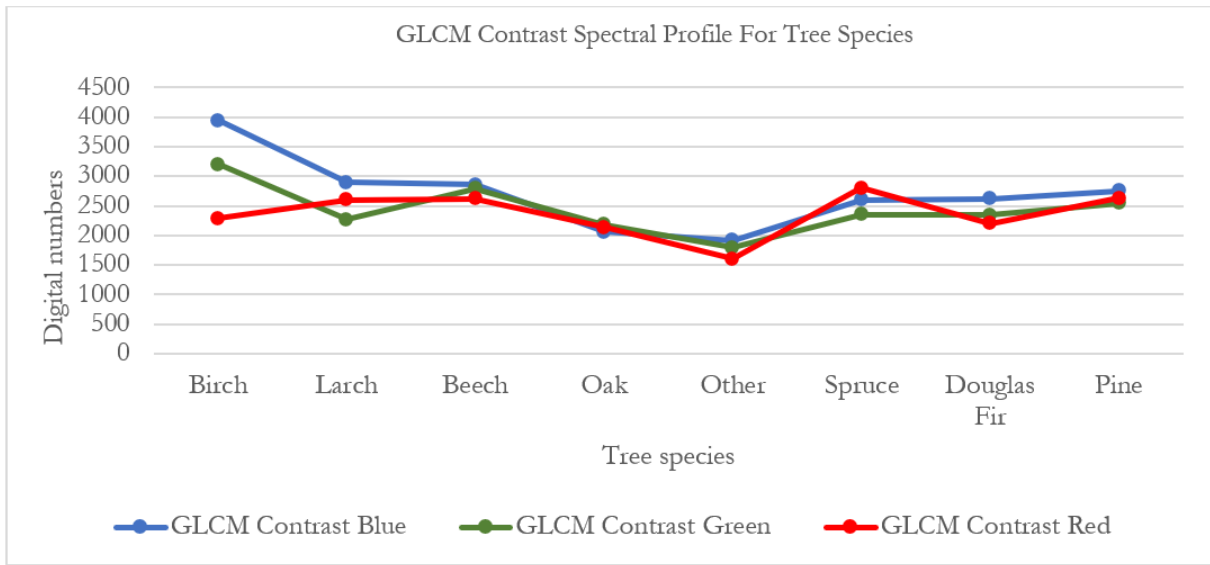


Figure 4-9: GLCM contrast spectral profile for tree species

Figure 4-9 above shows that the GLCM contrast of blue, green, and red has high separability for birch, indicating that birch trees can be classified with high accuracy compared to the other tree species in February when GLCM contrast is used.

4.3. UAV- MSS for tree species classification

The third and fourth research question is to investigate the accuracy of UAV-MSS and the combination of UAV-RGB and MSS. The results are discussed in 4.3.1 below.

4.3.1. UAV-MSS tree species classification

The UAV-MSS tree species classification produced an accuracy of 83% higher than all the seasonal UAV datasets. This result is inconsistent with research carried out by Michez et al. (2016) and Lisein et al. (2015), who compared RGB and MSS sensors for tree species classification and concluded that RGB outperforms the MSS dataset. Both studies commented that the poor performance of the MSS sensor could be attributed to the redundant sensitivity to NIR. The disparity can be attributed to the type of sensor used for the research. Michez et al. (2016) and Lisein et al. (2015) used a colour infrared (CIR) MSS sensor, which has three bands (green, red, and near-infrared). This study used a Sequoia camera that has four bands and does not experience the redundant sensitivity problem.

4.3.2. Combination of UAV-RGB and MSS tree species classification

The combination of UAV-RGB and UAV-MSS produced the highest overall accuracy of 88%. The accuracy obtained is lower than research carried out by Lisein et al. (2015), who classified tree species in a mixed forest and obtained an accuracy of 91.2. however, the accuracy is higher than the accuracy obtained by Michez et al. (2016), who obtained an accuracy of 84.1% when classifying tree species using the combination of UAV-RGB and UAV-MSS. Both studies considered five tree species classes, while this research considered eight tree species (7 individual images and the grouping of some tree species. The number of classes influences the accuracy of classification. The spectral confusion between classes become greater when the number of classes increases, and when some tree species show similar phenological changes over

the time period that the research was carried out (Michez et al., 2016). This research opted to identify the various tree species in the study area rather than choose a tree species sample that shows the best separation (Fassnacht et al., 2016).

Comparing the UAV-MSS tree species classification and the combination of UAV-RGB and MSS, the combination of UAV-RGB and MSS yielded a higher accuracy. Also, the F measure shows that UAV-RGB and MSS dataset had higher F measures for 5 of the eight tree species while the UAV-MSS had the highest F measure for the one tree species. The only difference between the UAV-MSS and the combination of RGB and MSS is the blue band; hence the blue band may be the reason for the increased inaccuracy. Research carried out by Grybas & Congalton (2021) to classify tree species remarked that the feature importance testing suggested that the blue band is very significant for tree species classification but not present in the MSS dataset. In their study, key et al. (2001) also identified the blue to be vital for tree species discrimination due to the sensitivity to chlorophyll and insensitivity to shadows (Milas et al., 2017).

5. CONCLUSION AND RECOMMENDATION

5.1. Conclusion

The research aimed to explore which seasonal dataset is best for tree species classification and examine the benefit of combining multi-spectral and RGB UAV images for tree species classification. The method used for this research included acquiring seasonal UAV images and tree species information. The UAV images were processed to obtain orthophoto, DSM, and DTM. Image segmentation was applied on the seasonal dataset to obtain the segment per season dataset. The created image segments were then used to extract features to be used for the classification. The field data was also split to training and validation samples. The optimal features per seasonal dataset were then used with the training data to classify the seasonal dataset. The accuracy of the seasonal tree species classification was then calculated.

Below are the conclusions per the research question and recommendations.

Question 1a. What are the segmentation accuracies of UAV-RGB seasonal datasets (winter, spring, summer, and fall)?

The winter dataset resulted in the highest segmentation error (i.e., 56%) and lowest accuracy of 46%. The spring dataset resulted in a segmentation error of 39% and an accuracy of 61%. The fall dataset generated a segmentation error of 21% and an accuracy of 79%. The summer dataset yielded the lowest segmentation error (19%) and accuracy of 81%.

Q1b. What is the segmentation accuracy of the UAV-MSS summer dataset?

The UAV-MSS dataset used for the image segmentation resulted in a segmentation error of 16% and an accuracy of 84%.

Q2. Which seasonal RGB dataset gives the highest classification accuracy separating individual tree species in the deciduous and coniferous forest?

The summer RGB produced the highest overall classification accuracy of 77% compared to the other seasonal RGB datasets. The summer RGB dataset produced the highest user accuracy for larch. The spring RGB dataset also produced the highest user accuracy for three tree species: beech, oak, and pine. The fall dataset also produced the highest user accuracy for birch and Douglas fir. Summer and fall RGB dataset produced equal accuracy for other while spring and summer RGB also produced an equal high accuracy for spruce.

Q3. What is the tree species classification accuracy for UAV-MSS imagery?

The overall tree species classification accuracy for the UAV-MSS dataset was 83%. However, the UAV-MSS dataset identified two tree species, namely pine and spruce, compared to the other dataset for tree species identification.

Q4. What is the accuracy for tree species classification in the combination of summer UAV-MSS and summer UAV-RGB?

The overall classification accuracy for the combination of Summer UAV-MSS and Summer UAV-RGB yielded the highest overall classification accuracy of 88%. Comparing all the datasets regarding tree species identification, the combination of UAV-RGB and UAV-MSS accurately identified five of the seven tree species. The tree species identified by the combination of UAV-RGB and UAV-MSS were Beech, Oak, Birch, Douglas Fir, and Spruce.

5.2. Recommendation

Tree species classification using RGB and MSS dataset for improved tree species classification provides further future study prospects. Based on the limitations encountered during this research, the following suggestions are recommended.

One of the most critical steps in this research was tree crown identification. The tree crowns (segments) are used to extract features from the input dataset. Hence, when the tree crowns are not correctly mapped, it results in extracting undesirable feature values, which affect the classification accuracy. Therefore, research should be carried out to map tree crowns (segments) using deep learning.

This research used the Support Vector Machine (SVM) classification algorithm to classify the tree species. UAV dataset is a very high-resolution image that can classify tree species using convoluted neural networks (CNN). CNN can be used to reduce the misclassification among some tree species. This can be achieved by generating sample patches that can improve class separability. Hence, research should be carried out using deep learning to classify the tree species.

Also, some tree species data used in the classification were few, which influences the classification output. Hence more field data for tree species such as chestnut, mountain ash, and Norway Marple should be collected. The tree species classification output may be influenced by the training and validation data's quality, quantity, and distribution.

eCognition Developer has some exciting features that may improve class separability, including geometry features (such as length/width, rectangular fit, and compactness of the image object) and class-related features (such as relation to neighbour objects). These features may help with species differentiation as some tree species has a specific crown.

LIST OF REFERENCES

- Abdollahnejad, A., & Panagiotidis, D. (2020). Tree species classification and health status assessment for a mixed broadleaf-conifer forest with uas multispectral imaging. *Remote Sensing*, 12(22), 1–21. <https://doi.org/10.3390/rs12223722>
- Aerts, R., & Honnay, O. (2011). Forest restoration, biodiversity and ecosystem functioning. *BMC Ecology*, 11(29). <https://doi.org/https://doi.org/10.1186/1472-6785-11-29>
- Alcantarilla, P. F., Bartoli, A., Davison, A. J., Fitzgibbon, A., Lazebnik, S., Perona, P., Sato, Y., & Schmid, C. (2012). KAZE Features. *Springer Berlin Heidelberg*, 214–227. https://doi.org/10.1007/978-3-642-33783-3_16
- Alkema, D., Bijker, W., Sharifa, A., Vekerdy, Z., Verhoef, W. (2013). Data Integration. In *The Core of GIScience: A systems-based approach* (pp. 206–213). University of Twente. <https://doi.org/10.1016/B978-0-12-385889-4.00013-2>
- Angelsen, A. (2001). Deforestation–Forestation. In P. B. B. Neil J. Smelser (Ed.), *International Encyclopedia of the Social & Behavioral Sciences* (pp. 3359–3364). Elsevier. <https://doi.org/10.1016/b0-08-043076-7/04173-5>
- Baatz, M., & Schäpe, A. (2000). Multiresolution Segmentation : an optimization approach for high quality multi-scale image segmentation. *Proceedings of Angewandte Geographische Informationsverarbeitung*, XII, 12–23. https://doi.org/10.1207/s15326888chc1304_3
- Bediako, P. A. (2020). The assessment of above ground biomass using a combination of Unmanned Aerial Vehicle (UAV) and the Aerial Laser Scanner (ALS). University of Twente.
- Bjerreskov, K. S., Nord-Larsen, T., & Fensholt, R. (2021). Classification of nemoral forests with fusion of multi-temporal sentinel-1 and 2 data. *Remote Sensing*, 13(5), 1–19. <https://doi.org/10.3390/rs13050950>
- Brandtberg, T. (2002). Individual tree-based species classification in high spatial resolution aerial images of forests using fuzzy sets. *Fuzzy Sets and Systems*, 132(3), 371–387. [https://doi.org/10.1016/S0165-0114\(02\)00049-0](https://doi.org/10.1016/S0165-0114(02)00049-0)
- Brus, D. J., Hengeveld, G. M., Walvoort, D. J. J., Goedhart, P. W., Heidema, A. H., Nabuurs, G. J., & Gunia, K. (2012). Statistical mapping of tree species over Europe. *European Journal of Forest Research*, 131(1), 145–157. <https://doi.org/10.1007/s10342-011-0513-5>
- Bruzzone, L., & Persello, C. (2009). Approaches based on support vector machine to classification of remote sensing data. In C. H. Chen (Ed.), *Handbook of Pattern Recognition and Computer Vision*, Fourth Edition (4th ed., pp. 329–352). World Scientific Press. https://doi.org/10.1142/9789814273398_014
- Cao, J., Leng, W., Liu, K., Liu, L., He, Z., & Zhu, Y. (2018). Object-Based Mangrove Species Classification Using Unmanned Aerial Vehicle Hyperspectral Images and Digital Surface Models. *Remote Sensing*, 10(89). <https://doi.org/10.3390/rs10010089>
- Carrio, A., Sampedro, C., Rodriguez-Ramos, A., & Campoy, P. (2017). A review of deep learning methods and applications for unmanned aerial vehicles. *Journal of Sensors*, 2017. <https://doi.org/10.1155/2017/3296874>
- Chang-Hua, J. U., Yong-Chao, T., Xia, Y., Wei-Xing, C., Zhu, Y., & Hannaway, D. (2010). Estimating Leaf Chlorophyll Content Using Red Edge Parameters * 1. In *Pedosphere* (Vol. 20, Issue 5). [https://doi.org/10.1016/S1002-0160\(10\)60053-7](https://doi.org/10.1016/S1002-0160(10)60053-7)
- Chen, S., Wang, W., Xu, W., Wang, Y., Wan, H., Chen, D., Tang, Z., Tang, X., Zhou, G., Xie, Z., Zhou, D., Shangguan, Z., Huang, J., He, J. S., Wang, Y., Sheng, J., Tang, L., Li, X., Dong, M., ... Bai, Y. (2018). Plant diversity enhances productivity and soil carbon storage. *Proceedings of the National Academy of Sciences of the United States of America*, 115(16), 4027–4032. <https://doi.org/10.1073/pnas.1700298114>
- Cho, M., Malahlela, O., & Ramoelo, A. (2015). Assessing the utility WorldView-2 imagery for tree species mapping in South African subtropical humid forest and the conservation implications: Dukuduku forest patch as case study. *International Journal of Applied Earth Observation and Geoinformation*, 38. <https://doi.org/10.1016/j.jag.2015.01.015>
- Clinton, N., Holt, A., Scarborough, J., Yan, L. I., & Gong, P. (2010). Accuracy assessment measures for object-based image segmentation goodness. *Photogrammetric Engineering and Remote Sensing*, 76(3), 289–299. <https://doi.org/10.14358/PERS.76.3.289>
- Congalton, R. G., & Green, K. (2019). *Assessing the Accuracy of Remotely Sensed Data: Principles and*

- Practices. In *Photogrammetric Engineering and Remote Sensing* (third Edition). CRC Press.
<https://books.google.nl/books?id=uvSDDwAAQBAJ>
- Data-flair. (2020). *Advantages and Disadvantages of Machine Learning Language - DataFlair*.
- Deur, M., Gašparović, M., & Balenović, I. (2020). Tree species classification in mixed deciduous forests using very high spatial resolution satellite imagery and machine learning methods. *Remote Sensing*, 12(23), 1–18. <https://doi.org/10.3390/rs12233926>
- Drăguț, L., Csillik, O., Eisank, C., & Tiede, D. (2014). Automated parameterisation for multi-scale image segmentation on multiple layers. *ISPRS Journal of Photogrammetry and Remote Sensing*, 88, 119–127. <https://doi.org/10.1016/j.isprsjprs.2013.11.018>
- Duncker, P. S., Raulund-Rasmussen, K., Gundersen, P., Katzensteiner, K., De Jong, J., Ravn, H. P., Smith, M., Eckmüller, O., & Spiecker, H. (2012, December). How forest management affects ecosystem services, including timber production and economic return: Synergies and trade-offs. *Ecology and Society; The Resilience Alliance*. <https://doi.org/10.5751/ES-05066-170450>
- Dymond, C. C., Mladenoff, D. J., & Radeloff, V. C. (2002). Phenological differences in Tasseled Cap indices improve deciduous forest classification. *Remote Sensing of Environment Environ*, 80, 460–472.
- eCognition. (2019). Basic rule set editing.
https://docs.ecognition.com/v9.5.0/eCognition_documentation/User_Guide_Developer/4_Basic_Rule_Set_Editing.htm
- eCognition. (2020). Calculating the nDSM. Trimble. <https://support.ecognition.com/hc/en-us/articles/360015556640-Calculating-the-nDSM>
- Edregosa, F., Varoquaux, G., Gramfort, A., Michel, V., Thirion, B., Grisel, O., Blondel, M., Prettenhofer, P., Weiss, R., Dubourg, V., Vanderplas, J., Passos, A., Cournapeau, D., Brucher, M., Perrot, M., & Duchesnay, E. (2011). Scikit-learn: Machine Learning in Python. *Journal of Machine Learning Research*, 12, 2825–2830. [https://scikit-learn.org/stable/auto_examples/svm/plot_rbf_parameters.html#:~:text=Intuitively%2C the gamma parameter defines,the model as support vectors.](https://scikit-learn.org/stable/auto_examples/svm/plot_rbf_parameters.html#:~:text=Intuitively%2C%20the%20gamma%20parameter%20defines%20the%20model%20as%20support%20vectors.)
- Erikson, M. (2004). Species classification of individually segmented tree crowns in high-resolution aerial images using radiometric and morphologic image measures. *Remote Sensing of Environment*, 91(3–4), 469–477. <https://doi.org/10.1016/j.rse.2004.04.006>
- Eshetae, M. A. (2020). Tree species classification using uav-rgb images and machine learning algorithms in a mixed temperate forest: a case study of haagse bos, netherlands [University of Twente]. <https://doi.org/10.1117/12.2531805>
- Esong Effiom, A. (2018). UAV-RGB and Multispectral Pleiades images, for tree species identification and forest carbon estimation in Amtsvenn, Germany. University of Twente.
- ESRI. (2016). Fundamentals of orthorectifying a raster dataset.
<http://desktop.arcgis.com/en/arcmap/10.3/manage-data/raster-and-images/fundamentals-oforthorectifying-a-raster-dataset.htm>
- FAO. (2020). Global forest resources assessment. <http://www.fao.org/3/I8661EN/i8661en.pdf>
- Fassnacht, F. E., Latifi, H., Stereńczak, K., Modzelewska, A., Lefsky, M., Waser, L. T., Straub, C., & Ghosh, A. (2016). Review of studies on tree species classification from remotely sensed data. *Remote Sensing of Environment*, 186, 64–87. <https://doi.org/10.1016/j.rse.2016.08.013>
- Fischler, M. ., & Bolles, R. C. (1987). Random sample consensus: a paradigm for model fitting with applications to image analysis and automated cartography. *Communications of the ACM*, 24(6), 381–395. <http://www.gisandbeers.com/RRSS/Publicaciones/Manual-Pix4D-Mapper.pdf>
- Franklin, S. E., Hall, R. J., Moskal, L. M., Maudie, A. J., & Lavigne, M. B. (2000). Incorporating texture into classification of forest species composition from airborne multispectral images. *International Journal of Remote Sensing*, 21(1), 61–79. <https://doi.org/10.1080/014311600210993>
- Gaden, K. (2020). Assessing potential of UAV multispectral imagery for estimation of AGB and carbon stock in conifer forest over UAV RGB imagery [University of Twente]. <http://essay.utwente.nl/85200/>
- Gao, Y., & Mas, J. F. (2008). A comparison of the performance of pixel-based and object-based classifications over images with various spatial resolutions.
- Gaston, K. J. (2000). Global patterns in biodiversity. In *Nature* (Vol. 405, Issue 6783, pp. 220–227). Nature Publishing Group. <https://doi.org/10.1038/35012228>
- Ghassemian, H. (2016). A review of remote sensing image fusion methods. *Information Fusion*, 32, 75–89. <https://doi.org/10.1016/j.inffus.2016.03.003>

- Gibbs, H. K., & Herold, M. (2007). Tropical deforestation and greenhouse gas emissions. *Environmental Research Letters*, 2(4). <https://doi.org/10.1088/1748-9326/2/4/045021>
- Glass, C. E. (2013). The near infra-red. In *Interpreting Aerial Photographs to Identify Natural Hazards* (1st ed., pp. 141–146). Elsevier. <https://doi.org/10.1016/B978-0-12-420018-0.00010-5>
- Grybas, H., & Congalton, R. G. (2021). A Comparison of Multi-Temporal RGB and Multispectral UAS Imagery for Tree Species Classification in Heterogeneous New Hampshire Forests. *Remote Sensing*, 13(2631).
- Haralick, R. M., Dinstein, I., & Shanmugam, K. (1973). Textural Features for Image Classification. *IEEE Transactions on Systems, Man and Cybernetics*, SMC-3(6), 610–621. <https://doi.org/10.1109/TSMC.1973.4309314>
- Heumann, B. W. (2011). An object-based classification of mangroves using a hybrid decision tree-support vector machine approach. *Remote Sensing*, 3(11), 2440–2460. <https://doi.org/10.3390/rs3112440>
- Hsu, C.-W., Chang, C.-C., & Lin, C.-J. (2003). A practical guide to support vector classification. In Department of Computer Science, National Taiwan University. <https://doi.org/10.1177/02632760022050997>
- Immitzer, M., Atzberger, C., & Koukal, T. (2012). Tree species classification with Random forest using very high spatial resolution 8-band worldView-2 satellite data. *Remote Sensing*, 4(9), 2661–2693. <https://doi.org/10.3390/rs4092661>
- Kachamba, D., Ørka, H., Gobakken, T., Eid, T., & Mwase, W. (2016). Biomass estimation using 3D data from Unmanned Aerial Vehicle imagery in a Tropical woodland. *Remote Sensing*, 8(11). <https://doi.org/10.3390/rs8110968>
- Kejriwal, L., & Singh, I. (2016). A Hybrid Filtering Approach of Digital Video Stabilization for UAV Using Kalman and Low Pass Filter. *Procedia Computer Science*, 93(September), 359–366. <https://doi.org/10.1016/j.procs.2016.07.221>
- Khazenie, N., & Richardson, K. (1993). Comparison of Texture Analysis Techniques in Both Frequency and Spatial Domains for Cloud Feature Extraction. *International Archives of Photogrammetry and Remote Sensing*, 29, 1009–1014.
- Kim, S., McGaughey, R. J., Andersen, H. E., & Schreuder, G. (2009). Tree species differentiation using intensity data derived from leaf-on and leaf-off airborne laser scanner data. *Remote Sensing of Environment*, 113(8), 1575–1586. <https://doi.org/10.1016/j.rse.2009.03.017>
- Landmap. (2021). Multi-Resolution Segmentation. <http://learningzone.rspsoc.org.uk/index.php/Learning-Materials/Object-oriented-Classification/2.5.-Multi-Resolution-Segmentation>
- Leyequien, E., Verrelst, J., Slot, M., Schaepman-Strub, G., Heitkönig, I. M. A., & Skidmore, A. (2007). Capturing the fugitive: Applying remote sensing to terrestrial animal distribution and diversity. In *International Journal of Applied Earth Observation and Geoinformation* (Vol. 9, Issue 1, pp. 1–20). Elsevier. <https://doi.org/10.1016/j.jag.2006.08.002>
- Lisein, J., Michez, A., Claessens, H., & Lejeune, P. (2015). Discrimination of deciduous tree species from time series of unmanned aerial system imagery. *PLoS ONE*, 10(11), 1–20. <https://doi.org/10.1371/journal.pone.0141006>
- M. F. Gomes, & Maillard, P. (2016). Detection of Tree Crowns in Very High Spatial Resolution Images. *Environmental Application of Remote Sensing*, 41–71. <https://doi.org/10.5772/62122>
- Mather, P., & Tso, B. (2016). *Classification Methods for Remotely Sensed Data* - Paul Mather, Brandt Tso - Google Books (2nd ed.). CRC Press.
- MathWork. (2020). Texture Analysis Using the Gray-Level Co-Occurrence Matrix (GLCM) - MATLAB & Simulink.
- MathWorks. (2020). Texture Analysis Using the Gray-Level Co-Occurrence Matrix (GLCM). [https://au.mathworks.com/help/images/texture-analysis-using-the-gray-level-co-occurrence-matrix-g lcm.html#:~:text=More About,Texture Analysis Using the Gray-Level Co-Occurrence Matrix \(gray-level spatial dependence matrix.](https://au.mathworks.com/help/images/texture-analysis-using-the-gray-level-co-occurrence-matrix-g lcm.html#:~:text=More About,Texture Analysis Using the Gray-Level Co-Occurrence Matrix (gray-level spatial dependence matrix.)
- Michez, A., Piégay, H., Lisein, J., Claessens, H., & Lejeune, P. (2016). Classification of riparian forest species and health condition using multi-temporal and hyperspatial imagery from unmanned aerial system. *Environmental Monitoring and Assessment*, 188(3), 1–19. <https://doi.org/10.1007/s10661-015-4996-2>
- Mickelson, J. G., Civco, D. L., & Silander, J. A. (1998). Delineating forest canopy species in the northeastern United States using multi-temporal TM imagery. *Photogrammetric Engineering and Remote Sensing*, 64(9), 891–904.

- Milas, A., Arend, K., AMayer, C., Simonson, M. A., & Mackey, S. (2017). Different colours of shadows: classification of UAV images. *International Journal of Remote Sensing*, 38, 8–10. <https://doi.org/doi:10.1080/01431161.2016.1274449>
- Modzelewska, A., Fassnacht, F. E., & Stereńczak, K. (2020). Tree species identification within an extensive forest area with diverse management regimes using airborne hyperspectral data. *International Journal of Applied Earth Observation and Geoinformation*, 84, 101960. <https://doi.org/10.1016/j.jag.2019.101960>
- Möller, M., Lymburner, L., & Volk, M. (2007). The comparison index: A tool for assessing the accuracy of image segmentation. *International Journal of Applied Earth Observation and Geoinformation*, 9(3), 311–321. <https://doi.org/https://doi.org/10.1016/j.jag.2006.10.002>
- Mryka Hall-Beyer, P. D. (2017). GLCM Texture: A Tutorial. In 17th International Symposium on Ballistics (Vol. 2, Issue March).
- Nagendra, H. (2001). Using remote sensing to assess biodiversity. *International Journal of Remote Sensing*, 22(12), 2377–2400. <https://doi.org/10.1080/01431160117096>
- Näsi, R., Honkavaara, E., Tuominen, S., Saari, H., Pölönen, I., Hakala, T., Viljanen, N., Soukkamäki, J., Näkki, I., Ojanen, H., & Reinikainen, J. (2016). Uas based tree species identification using the novel FPI based hyperspectral cameras in visible, nir and swir spectral ranges. *International Archives of the Photogrammetry, Remote Sensing and Spatial Information Sciences - ISPRS Archives*, 2016-Janua(July), 1143–1148. <https://doi.org/10.5194/isprsarchives-XLI-B1-1143-2016>
- Natesan, S., Armenakis, C., & Vepakomma, U. (2019). Resnet-based tree species classification using uav images. *International Archives of the Photogrammetry, Remote Sensing and Spatial Information Sciences - ISPRS Archives*, 42(2/W13), 475–481. <https://doi.org/10.5194/isprs-archives-XLII-2-W13-475-2019>
- National, G. (2021). Season. <https://www.nationalgeographic.org/encyclopedia/season/#:~:text=The four seasons—spring%2C summer,weather patterns that repeat yearly.>
- Natuurmonumenten. (2021). A Movement for Movement. <https://www.natuurmonumenten.nl/visie>
- Nevalainen, O., Honkavaara, E., Tuominen, S., Viljanen, N., Hakala, T., Yu, X., Hyypä, J., Saari, H., Pölönen, I., Imai, N. N., & Tommaselli, A. M. G. (2017). Individual tree detection and classification with UAV-Based photogrammetric point clouds and hyperspectral imaging. *Remote Sensing*, 9(3). <https://doi.org/10.3390/rs9030185>
- Nex, F., & Remondino, F. (2014). UAV for 3D mapping applications: A review. *Applied Geomatics*, 6(1), 1–15. <https://doi.org/https://doi.org/10.1007/s12518-013-0120-x>
- Obeng-Manu, C. (2019). Assessing the accuracy of UAV-DTM generated under different forest canopy density and its effect on estimation of aboveground carbon in Asubima forest, Ghana. (Master's Thesis Universty of Twente, Enschede, The Netherlands: Faculty ITC).
- Okojie, J. A. (2017). Assessment of Forest Tree Structural Parameter Extractability From Optical Imaging Uav Datasets , in Ahaus. Germany. The University of Twente, Faculty of Geo-information and Earth Observation Science(ITC) MSc thesis. R. (Issue May) [University of Twente]. https://www.researchgate.net/publication/316734569_ASSESSMENT_OF_FOREST_TREE_STRUCTURAL_PARAMETER_EXTRACTABILITY_FROM_OPTICAL_IMAGING_UAV_DATASETS_IN_AHAUS_GERMANY%0Ahttps://webapps.itc.utwente.nl/librarywww/papers_2017/msc/nrm/okojie.pdf
- Onishi, M., & Ise, T. (2018). Automatic classification of trees using a UAV onboard camera and deep learning.
- Overpeck, J., Garfin, G., Jardine, A., Busch, D. E., Cayan, D., Dettinger, M., Fleishman, E., Gershunov, A., MacDonald, G., Redmond, K. T., Travis, W. R., & Udall, B. (2005). Ecosystems and human well-being. In Island Press. https://doi.org/10.5822/978-1-61091-484-0_1
- Persson, M., Lindberg, E., & Reese, H. (2018). Tree species classification with multi-temporal Sentinel-2 data. *Remote Sensing*, 10(11), 1–17. <https://doi.org/10.3390/rs10111794>
- Pix4D. (2020). Processing options. <https://support.pix4d.com/hc/en-us/articles/202557759-Menu-Process-Processing-Options-1-Initial-Processing-General>
- Pix4D. (2021). Tie points in photogrammetry project (ATP, GCP, MTP, and CP). <https://support.pix4d.com/hc/en-us/articles/115000140963-Tie-points-in-photogrammetry-project-ATP-GCP-MTP-and-CP>
- Pix4D S.A. (2017). Pix4Dmapper user manuel. <https://support.pix4d.com/hc/en-us/sections/360003718992-Manual>
- Pu, R., & Landry, S. (2012). A comparative analysis of high spatial resolution IKONOS and WorldView-2

- imagery for mapping urban tree species. *Remote Sensing of Environment*, 124, 516–533. <https://doi.org/https://doi.org/10.1016/j.rse.2012.06.011>
- Rocheleau, S. (2009). Oak vs. Beech. <https://www.hunker.com/12555811/cherry-vs-oak-hardwood-comparison>
- Sahu, D. K., & Parsai, M. P. (2012). Different Image Fusion Techniques – A critical review. 2, 4298–4301.
- Schwenk, W. S., Donovan, T. M., Keeton, W. S., & Nunery, J. S. (2012). Carbon storage, timber production, and biodiversity: Comparing ecosystem services with multi-criteria decision analysis. *Ecological Applications*, 22(5), 1612–1627. <https://doi.org/10.1890/11-0864.1>
- senseFly. (2021). Parrot Sequoia+ Multispectral Camera. <https://www.sensefly.com/camera/parrot-sequoia/>
- Sheeren, D., Fauvel, M., Josipovi, V., Lopes, M., Planque, C., Willm, J., & Dejoux, J.-F. (2016). [July, 2020]. *Remote Sensing*, 8(734), 63. <https://doi.org/10.3390/rs8090734>
- Sheeren, D., Fauvel, M., Josipović, V., Lopes, M., Planque, C., Willm, J., & Dejoux, J. F. (2016). Tree species classification in temperate forests using Formosat-2 satellite image time series. *Remote Sensing*, 8(9), 1–29. <https://doi.org/10.3390/rs8090734>
- Shimadzu, H., Dornelas, M., Henderson, P. A., & Magurran, A. E. (2013). Diversity is maintained by seasonal variation in species abundance. *BMC Biology*, 11(1), 98. <https://doi.org/10.1186/1741-7007-11-98>
- Snavely, N., Seitz, S. M., & Szeliski, R. (2008). Modeling the world from internet photo collections. *International Journal of Computer Vision*, 80(2), 189–210. <https://doi.org/https://doi.org/10.1007/s11263-007-0107-3>
- Sothe, C., Dalponte, M., de Almeida, C. M., Schimalski, M. B., Lima, C. L., Liesenberg, V., Miyoshi, G. T., & Tommaselli, A. M. G. (2019). Tree species classification in a highly diverse subtropical forest integrating UAV-based photogrammetric point cloud and hyperspectral data. *Remote Sensing*, 11(11). <https://doi.org/10.3390/rs11111338>
- Tenaw, W. (2011). Assessment of aboveground carbon stock in coniferous and broadleaf forests, using high spatial resolution satellite images. University of Twente.
- Viennois, G., Proisy, C., Féret, J. B., Prosperi, J., Sidik, F., Suhardjono, Rahmania, R., Longépé, N., Germain, O., & Gaspar, P. (2016). Multitemporal Analysis of High-Spatial-Resolution Optical Satellite Imagery for Mangrove Species Mapping in Bali, Indonesia. *IEEE Journal of Selected Topics in Applied Earth Observations and Remote Sensing*, 9(8), 3680–3686. <https://doi.org/10.1109/JSTARS.2016.2553170>
- Wang, D., Wan, B., Qiu, P., Su, Y., Guo, Q., & Wu, X. (2018). Artificial Mangrove Species Mapping Using Pléiades-1: An Evaluation of Pixel-Based and Object-Based Classifications with Selected Machine Learning Algorithms. *Remote Sensing*, 10(2), 294. <https://doi.org/10.3390/rs10020294>
- Weih, R. C., & Riggan, N. (2010). Object-based classification vs. pixel-based classification: Comparative importance of multi-resolution imagery. *The International Archives of the Photogrammetry, Remote Sensing and Spatial Information Sciences*, XXXVIII, 1–6.
- Weil, G., Lensky, I. M., Resheff, Y. S., & Levin, N. (2017). Optimizing the timing of unmanned aerial vehicle image acquisition for applied mapping of woody vegetation species using feature selection. *Remote Sensing*, 9(11). <https://doi.org/10.3390/rs9111130>
- Westoby, M. J., Brasington, J., Glasser, N. F., Hambrey, M. J., & Reynolds, J. M. (2012). “Structure-from-Motion” photogrammetry: A low-cost, effective tool for geoscience applications. *Geomorphology*, 179, 300–314. <https://doi.org/10.1016/j.geomorph.2012.08.021>
- Xie, Z., Chen, Y., Lu, D., Li, G., & Chen, E. (2019). Classification of Land cover, Forest, and Tree species Classes with ZiYuan-3 Multispectral and Stereo Data. *Remote Sensing*, 11(164). <https://doi.org/10.3390/rs11020164>
- Xie, Zhuli, Chen, Y., Lu, D., Li, G., & Chen, E. (2019). Classification of land cover, forest, and tree species classes with Ziyuan-3 multispectral and stereo data. *Remote Sensing*, 11(2). <https://doi.org/10.3390/rs11020164>
- Xu, Z., Shen, X., Cao, L., Coops, N. C., Goodbody, T. R. H., Zhong, T., Zhao, W., Sun, Q., Ba, S., Zhang, Z., & Wu, X. (2020). Tree species classification using UAS-based digital aerial photogrammetry point clouds and multispectral imageries in subtropical natural forests. *International Journal of Applied Earth Observation and Geoinformation*, 92, 102173. <https://doi.org/10.1016/j.jag.2020.102173>
- Yang, G., Zhao, Y., Li, B., Ma, Y., Li, R., Jing, J., & Dian, Y. (2019). Tree species classification by employing multiple features acquired from integrated sensors. *Journal of Sensors*, 2019.

<https://doi.org/10.1155/2019/3247946>

- Yao, H., Qin, R., & Chen, X. (2019). Unmanned aerial vehicle for remote sensing applications - A review. In *Remote Sensing* (Vol. 11, Issue 12, p. 1443). MDPI AG. <https://doi.org/10.3390/rs11121443>
- ZhiYong, L. , Shi, W., Benediktsson, J. A., & Gao, L. (2018). A modified mean filter for improving the classification performance of very high-resolution remote-sensing imagery. *International Journal of Remote Sensing*, 39(3), 770–785. <https://doi.org/10.1080/01431161.2017.1390275>
- Zhu, H., Cai, L., Liu, H., & Huang, W. (2016). Information extraction of high resolution remote sensing images based on the calculation of optimal segmentation parameters. *PLoS ONE*, 11(6), 1–15. <https://doi.org/10.1371/journal.pone.0158585>

APPENDICES

Appendix 1: Recoded field data for classification

Category	Tree species	Scientific name	Classification code
Broadleaved	European white birch	<i>Betula pendula</i>	1
	European red beech	<i>Fagus sylvatica</i>	8
	European beech	<i>Fagus sylvatic</i>	2
	Chestnut	<i>Castanea sativa</i>	8
	Mountain ash	<i>Sorbus aucuparia</i>	8
	Oak	<i>Quercus robur</i>	3
Coniferous	Scot pine	<i>Pinus sylvestris</i>	4
	European larch	<i>Larix decidua</i>	5
	Douglas fir	<i>Pseudotsuga menziesii</i>	6
	Norway Spruce	<i>Picea abies</i>	7
Non-tree	-	-	9

Appendix 2: Spectral and texture features available in eCognition.

Data	Features
RGB seasonal data	<p>Mean of Red, Green, Blue, and CHM; Standard deviation of Red, Green, Blue, and CHM; GLCM contrast of Red, Green, Blue, and CHM; GLCM correlation of Red, Green, Blue, and CHM; GLCM dissimilarity of Red, Green, Blue, and CHM; GLCM entropy of Red, Green, Blue, and CHM; GLCM mean of Red, Green, Blue, and CHM; GLCM standard deviation of Red, Green, Blue, and CHM; GLDV contrast of Red, Green, Blue, and CHM; GLDV entropy of Red, Green, Blue, and CHM, GLDV mean of Red, Green, Blue, CHM</p>
MSS seasonal data	<p>Mean of Green, Red, Red edge, NIR, CHM; Standard deviation of Green, Red, Red edge, NIR, CHM; GLCM contrast of Green, Red, Red edge, NIR, CHM; GLCM correlation (Green, Red, Red edge, NIR, CHM), GLCM dissimilarity (Green, Red, Red edge, NIR, CHM), GLCM entropy (Green, Red, Red edge, NIR, CHM), GLCM mean (Green, Red, Red edge, NIR, CHM), GLCM standard deviation (Green, Red, Red edge, NIR, CHM), GLDV contrast (Green, Red, Red edge, NIR, CHM), GLDV entropy (Green, Red, Red edge, NIR, CHM), GLDV mean (Green, Red, Red edge, NIR, CHM)</p>

MSS and RGB dataset combination	Mean (Blue, Green, Red, Red edge, NIR, CHM), standard deviation (Blue, Green, Red, Red edge, NIR, CHM), GLCM contrast (Blue, Green, Red, Red edge, NIR, CHM), GLCM correlation (Blue, Green, Red, Red edge, NIR, CHM), GLCM dissimilarity (Blue, Green, Red, Red edge, NIR, CHM), GLCM entropy (Blue, Green, Red, Red edge, NIR, CHM), GLCM mean (Blue, Green, Red, Red edge, NIR, CHM), GLCM standard deviation (Blue, Green, Red, Red edge, NIR, CHM), GLDV contrast (Blue, Green, Red, Red edge, NIR, CHM), GLDV entropy (Blue, Green, Red, Red edge, NIR, CHM), GLDV mean (Blue, Green, Red, Red edge, NIR, CHM)
---------------------------------	--

Appendix 3: Spectral and texture features per seasonal dataset for classification.

Data type	Dataset	Features
RGB	Winter	Mean (red, green, blue, CHM) Standard deviation (red, green, blue, CHM) GLCM contrast (blue, red, CHM) GLCM mean (red, green, blue) CHM), GLDV entropy (red, green, blue, CHM)
	Spring	Mean (red, green, blue, CHM) Standard deviation (red, green, blue, CHM) GLCM dissimilarity (red, green, blue) GLCM contrast (red, blue, CHM)
	Summer	Mean (red, green, blue, CHM) Standard deviation (red, green, blue, CHM) GLCM entropy (red, green, blue, CHM) GLDV contrast (red, green, blue, CHM)
	Spring	Mean (red, green, blue, CHM), Standard deviation (red, green, blue, CHM) GLCM contrast (blue, red) GLCM mean (red, green, blue, CHM), GLCM entropy (red, green, blue, CHM) GLDV mean (red, green, blue, CHM) GLCM standard deviation (red, green, blue, CHM)
MSS	Summer	Mean (red, green, near infra-red, red edge, CHM) Standard deviation (red, green, near infra-red, red-edge, CHM) GLCM entropy (red, green, CHM) GLCM mean (red, green, near infra-red, CHM) GLDV contrast (red, green, CHM)
Combination	Summer MSS and RGB	Mean (blue, red, green, near infra-red, red edge, CHM) standard deviation (blue, red, green, near infra-red, red-edge, CHM), GLCM entropy (red, near infra-red), GLCM mean (blue, CHM), GLDV contrast (blue, green, CHM)